UCRL-10530

University of California

Ernest O. Lawrence
Radiation Laboratory

STUDY OF PION-PION SCATTERING FROM THE REACTION $\pi^+ + p \rightarrow \pi^+ + \pi^+ + n$ AT 1.25 AND 1.75 BeV/c

Berkeley, California

DISCLAIMER

UCRL-10530
UC-34 Physics
TID-4500 (18th Ed.)

UNIVERSITY OF CALIFORNIA

Lawrence Radiation Laboratory
Berkeley, California

Contract No. W-7405-eng-48

STUDY OF PION-PION SCATTERING FROM THE REACTION $\pi^+ + p \rightarrow \pi^+ + \pi^+ + n$ AT 1.25 AND 1.75 BeV/c

Leonard B. Auerbach

(Ph. D. Thesis)

October 31, 1962

Printed in USA. Price $1.75. Available from the
Office of Technical Services
U. S. Department of Commerce
Washington 25, D.C.

STUDY OF PION-PION SCATTERING FROM THE REACTION $\pi^+ + p \rightarrow \pi^+ + \pi^+ + n$ AT 1.25 AND 1.75 BeV/c

Contents

THIS PAGE

WAS INTENTIONALLY

LEFT BLANK

STUDY OF PION-PION SCATTERING FROM THE REACTION $\pi^+ + p \rightarrow \pi^+ + \pi^+ + n$ AT 1.25 AND 1.75 BeV/c

Leonard B. Auerbach

Lawrence Radiation Laboratory
University of California
Berkeley, California

October 31, 1962

ABSTRACT

The distribution in energy and angle of recoil neutrons from the reaction $\pi^+ + p \rightarrow \pi^+ + \pi^+ + n$ was measured for incident-pion laboratory momenta of 1.25 and 1.75 BeV/c. The investigation was limited to events in which the momentum transfer to the neutron was in the range 95 to 355 MeV/c. The detection apparatus consisted entirely of plastic scintillation counters and was divided into two groups. The forward group (4° to 60°) detected both pions and neutrons. The other group (60° to 145°) detected pions only. A time-of-flight measurement on the neutron was used to determine its energy. The data were stored on magnetic tapes and analyzed by suitable programming for an IBM 7090 computer.

The purpose of the experiment was to determine the cross section for pion-pion scattering at a number of energies. The method to be used was the extrapolation procedure formulated by G. Chew and F. Low. The Yang-Treiman test was applied to the data and showed deviation from single-pion exchange for those events in which the neutrons had energies in the upper part of the energy range investigated. Analysis of the data in terms of number of events vs final-state pion-neutron barycentric energy showed peaking of the distributions at the (3/2, 3/2) and (1/2, 3/2) pion-nucleon resonances for the 1.25 BeV/c data. At 1.75 BeV/C, peaking occurred at the (3/2, 3/2) and (1/2, 5/2) resonances. The extrapolation method applied to our data appeared to fail, in the sense that the pion-pion cross sections obtained were very small (consistent with zero,

within the errors) or were negative. From the distribution of events as a function of pion-pion barycentric energy, there was no indication of a pion-pion resonance (I-spin 2) in the energy interval investigated in this experiment.

I. INTRODUCTION

It has been recognized for many years that a thorough knowledge of the interaction of pions with other particles would be of great value in building a theory of elementary particles. To obtain such knowledge, the main avenue of approach has been the investigation of the scattering of pions in a beam from targets composed only of those particles whose interactions with pions were to be studied. Thus, for example, the pion-proton interaction has been sought by studying pion scattering from a hydrogen target. Since neutron targets are not available, the pion-neutron interaction cannot be studied in this manner. Even in the simplest target system containing neutrons (deuterium), the neutrons are bound in the target, and although one can distinguish between the pion-neutron and pion-proton scatterings, the neutron-proton binding forces influence the observed pion-neutron cross section. One would have to know the binding forces and the way in which they interfere with the pion-neutron forces in order to isolate the pion-neutron interaction. In a somewhat similar way, if one wanted to study the pion-pion interaction, the difficulty arising from the unavailability of pion targets might be overcome by scattering pions in a beam from pions virtually contained in a proton target, e.g., by the reaction

$$\text{pion} + \begin{pmatrix} \text{nucleon} \\ \text{virtual pion}^{\pm} \end{pmatrix} \rightarrow \text{nucleon} + \text{pion} + \text{pion}.$$

Here, again, one would have to know how to calculate the contribution of the pion-nucleon binding in the target to the observed scattering cross section.

In 1959, Chew and Low[1] suggested a method for overcoming the complications arising from binding between particles in a complex target. The ideas that provided a basis for their approach are given in detail in their paper and elsewhere.[2] It was their proposal for determination of the pion-pion cross section that prompted us to do the

experiment reported in this paper. It was hoped that, for small four-momentum transfer between target and recoil nucleon, the dominant contribution to the reaction $\pi + N \rightarrow \pi + \pi + N'$ would be from the exchange of a single pion between target and incident particle. The differential cross section for this process could be calculated through a knowledge of the singularities (poles) in the scattering amplitude as a function of the four-momentum-transfer variable $p_{\text{virtual pion}} = p_{\text{target}} - p_{\text{recoil nucleon}}$.

The essential feature of the analysis was that the scattering amplitude would, in the neighborhood of $p^2 = -\mu^2$, be dominated by the pole term arising from single-pion exchange to the extent that the differential cross section for the reaction $\pi + N \rightarrow 2\pi + N$ could be determined without a knowledge of the other terms in the amplitude. The assumptions were that there be no other terms in p^2 having poles near $p^2 = -\mu$ and that terms from the interference between analytic (in p^2) parts in the amplitude and the single-pion pole term be small.

This author chose to study the reaction $\pi^+ + p \rightarrow \pi^+ + \pi^+ + n$ in order to find the cross section for $\pi^+ + \pi^+ \rightarrow \pi^+ + \pi^+$. This scattering takes place in a pure isotopic spin-2 state, and it was hoped that the data obtained taken together with data on other I-spin states would help to develop a general picture of the pion-pion interaction.

The Chew-Low (CL) analysis is based on the assumption that the scattering is dominated by the exchange of a single pion between the target and the incident particle for those scatterings in which the four-momentum transfer to the recoil nucleon is small. The Feynman diagram for this process is shown in Fig. 1. Following the notation of CL, we define

μ = mass of the pion,
M_p = mass of the target proton,
M_n = mass of the neutron,
q_{1L} = momentum of the incident pion,
ω_{1L} = energy of the incident pion,
p_{2L} = momentum of the neutron,
T_{2L} = kinetic energy of the neutron,

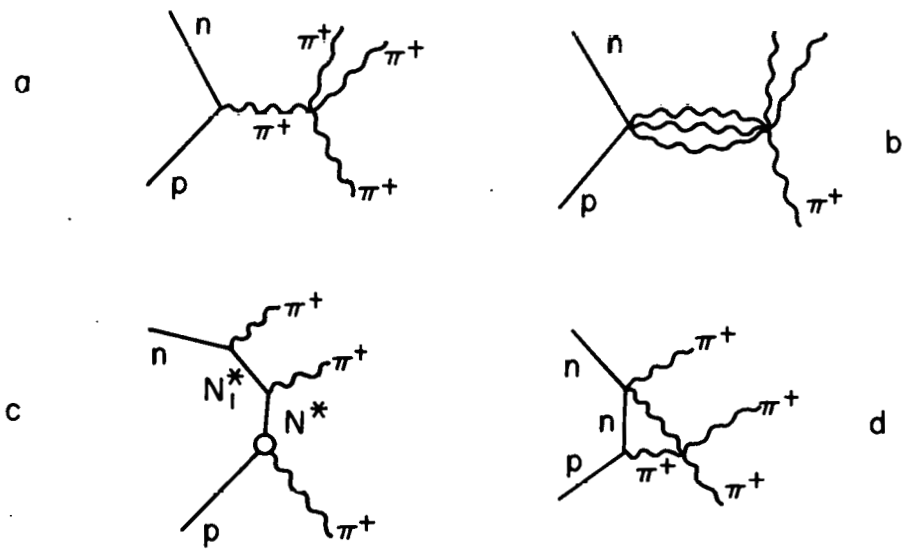

MU-28802

Fig. 1. Feynman diagrams for single-pion production via (a) single-pion exchange, (b) three-pion exchange, (c) isobar formation, (d) single-pion exchange with a final-state pion-nucleon interaction.

and

θ_{2L} = angle between incident pion and recoil neutron.

The subscript L refers to the laboratory frame of reference. Let p_1, p_T, p_n, p_3, and p_4 be the four-momenta of the incident particle, target proton, recoil neutron and final-state pions, respectively.

We are interested in the variables ω^2 (the square of the dipion barycentric energy) and Δ^2 (the square of the four-momentum transfer between target and recoil nucleon). Thus,

$$\begin{aligned}\omega^2 &= (p_3 + p_4)^2 = p_T - p_n)^2 \\ &= (\omega_{1L} + M_p - M_n - T_{2L})^2 - (q_{1L}^2 + p_{2L}^2 - 2q_{1L}p_{2L}\cos\theta_{2L}), \\ \Delta^2 &= (p_T - p_n)^2 = 2M_p T_{2L} - (M_p - M_n)^2,\end{aligned}$$

and

$$p^2 = 2M_n T_{2L} = (M_n/M_p)[\Delta^2 + (M_p - M_n)^2].$$

From the experimental determination of the cross section for scattering neutrons per unit interval of p^2 and ω^2[(denoted by $\partial^2\sigma/\partial p^2 \partial\omega^2$)], one obtains the pion-pion cross section from the equation

$$\lim_{p^2 \to -\mu^2} \frac{\partial^2\sigma}{\partial p^2 \partial\omega^2} \to \frac{M_n^2}{M_p^2} \frac{f^2}{\pi} \frac{1}{q_{1L}^2} \frac{p^2/\mu^2}{(p^2+\mu^2)^2} \omega\left(\frac{\omega^2}{4} - \mu^2\right)^{1/2} \sigma_{\pi\pi}(\omega), \qquad (I\text{-}1)$$

where $f^2 = 0.08$ is the pion-nucleon coupling constant.

For all physical measurements, $p^2 > 0$. This can be seen from its definition as the nonrelativistic expression for the momentum squared of the neutron, i.e., $p^2 = 2M_n T_{2L}$. If, however, the variable is allowed to take on negative values, then for $p^2 = -\mu^2$ the expression for $\partial^2\sigma/\partial p^2 \partial\omega^2$ becomes infinite owing to the presence of the term $1/(p^2+\mu^2)^2$. Since Eq. (I-1) is defined to hold in the limit as $p^2 \to -\mu^2$, we can construct the function

$$F(p^2, \omega^2) = (p^2+\mu^2)^2 \frac{\partial^2\sigma}{\partial p^2 \partial\omega^2} \left(\frac{M_p}{M_n}\right)^2 \frac{\pi}{f^2} q_{1L}^2 \frac{1}{\omega\left(\frac{\omega^2}{4} - \mu^2\right)^{1/2}},$$

and expand it in a power series in p^2 about the point $p^2 = -\mu^2$:

$$F(p^2, \omega^2) = a_0 + a_1(p^2 + \mu^2) + a_2(p^2 + \mu^2)^2 + \cdots .$$

If this expression is evaluated at $p^2 = -\mu^2$, the coefficient a_0 is then just equal to the desired cross section $\sigma_{\pi\pi}(\omega)$. To determine the range in p^2 over which the expansion is allowable, note that if the reaction $\pi^+ + p \rightarrow \pi^+ + \pi^+ + n$ were to proceed via the exchange of three pions [see Fig. 1(b)], there would be a branch cut along the negative p^2 axis extending from the value of the lightest mass exchanged to infinity. The lightest mass is 3μ, so that the nearest singularity is at $-9\mu^2$. Thus, if the reaction $\pi^+ + p \rightarrow \pi^+ + \pi^+ + n$ is studied by detecting neutrons with values of $p^2 > 0$ as close as possible to the point $p^2 = -\mu^2$, the single-pion exchange pole should be the dominant one, and the evaluation of the coefficient a_0 should yield $\sigma_{\pi\pi}$.

In using this extrapolation procedure, there is no way of knowing what the order of the polynomial should be. Chew suggested that for $p^2 < (300\ \mathrm{MeV}/c)^2$ (KE $\approx$ 47 MeV), the best-fit polynomial should be at most a cubic, and to determine the correct polynomial order one should attempt linear, quadratic, cubic, and higher fits.[3] If a plateau in the value of $\sigma_{\pi\pi}$ is obtained from two or three consecutive polynomials, then one has experimentally determined the correct polynomial order. Such a program is difficult to carry out because one would need data at many values of p^2, and one would need good statistics on the points.

It should be emphasized at this point that if $F(p^2, \omega^2)$ were to turn out to be linear in p^2, i.e., $F(p^2, \omega^2) = a_0 + a_1(p^2 + \mu^2)$, and if $F(0, \omega^2) = 0$, then one would not need to carry out an extrapolation in order to determine $\sigma_{\pi\pi}$, or, what is an equivalent statement, Eq. (1) would be an exact equation for $p^2 \geq 0$ rather than a relation that holds true only in the limit $p^2 \rightarrow -\mu^2$. Then $\sigma_{\pi\pi}(\omega)$ could be obtained by intergrating Eq. (1) over p^2 within appropriate limits. It should also be made clear that if single-pion production goes via the isobar model,[4] i.e., $\pi^+ + p \rightarrow N^* \rightarrow N_1^* + \pi$, $N_1^* \rightarrow N + \pi$ (see Fig. 1c), or if there is a final-state pion-nucleon interaction (see Fig. 1d), the extrapolation procedure may not work at all.

II. EXPERIMENT

A. Introduction

The work reported in this paper was part of a joint effort to investigate the reactions $\pi^- + p \rightarrow \pi^\pm + \pi^+ + n$ and $p + p \rightarrow p + \pi^+ + n$ by using plastic scintillation counters as particle detectors.[5] We decided to study these reactions rather than the set $\pi^\pm + p \rightarrow \pi^\pm + \pi^0 + p$ and $p + p \rightarrow p + \pi^+ + \pi^0$ because of the difficulty of extracting low-energy protons ($T_{proton} \leq 50$ MeV) from a liquid hydrogen target. Although the detection efficiency for protons is essentially 100% in plastic scintillation counters, this advantage would be offset by the short range of the protons and by the multiple scattering and energy loss that they would undergo in traversing any material between target and detector, thereby masking both the initial angle and energy they had just after collision.

The efficiency for detecting neutrons with plastic scintillation counters is a function of the size, geometry, and light-collection efficiency of the counters. We chose to use 15-cm-thick counters so that our efficiency would be approx 25% over a large part of the kinetic energy interval 5 to 50 MeV.[6] To determine the neutron energy, we decided to measure the time of flight of the neutron between hydrogen target and detection counter. From kinematic considerations on the range of the dipion energy ω to be investigated, the maximum detection angle for scattered neutrons was chosen as 60° and the incident momenta as 1.25 and 1.75 BeV/c. The determination of 4° as the minimum detection angle was made on the basis of beam design and target size.[7] To insure that both pions from a scattering would be detected, an array of counters was used for pions scattered between 60° and 147°. The decision made about the angular intervals to be subtended by each counter was the result of a compromise between the desired resolution of the data as a function of p^2 and ω^2, the limitations based on size and cost of equipment, and the amount of electronics needed to handle the information coming from the counters.

For the lower energies of the p^2 spectrum, we had to have enough signal from the counters to distinguish reliably between signal and noise pulses. Also, when one makes a choice of reaction and incident momentum, the kinematics sets the lower limit on p^2 for a given ω^2. Once more, the choice of a lower limit on p^2 is a compromise between what is desired from the physics aspect and what is experimentally feasible.

We chose to measure the differential cross section for recoil neutrons with energies in the interval $6 < T_{2L} < 57$ MeV. The corresponding flight-time interval $\Delta\tau$ for a 160-cm path is $48 > \Delta\tau > 16$ nsec. We decided to divide this into seven parts, $\Delta\tau_j$. (These increments $\Delta\tau_j$ are referred to as "time bins.") To each time bin would correspond a mean neutron energy E_j, and our cross-section measurement would consist, essentially, of determining the number of scattered neutrons at each of the seven energies E_j. The time boundaries of these bins are given in Table I. Also included in the table are the neutron kinetic energies corresponding to those flight times for a 160-cm path. The method used to determine the mean value of the energy and the rms spread in energy for each bin is given in Section IIE.

Table I. The nominal neutron flight times τ_n and kinetic energies T_{2L} for the seven time bins.

Bin No.	min τ_n (nsec)	max τ_n (nsec)	max T_{2L} (MeV)	min T_{2L} (MeV)
1	16.0	18.8	57.0	40.3
2	18.8	21.9	40.3	29.2
3	21.9	25.6	29.2	21.1
4	25.6	29.9	21.1	15.3
5	29.9	34.4	15.3	11.5
6	34.4	40.8	11.5	8.1
7	40.8	47.8	8.1	5.9

The circuitry in which the time measuring was done will be referred to as the "chronotron" and is described in reference 8. The chronotron compared the neutron flight time with that of a particle with $\beta = 1$. The start pulse, serving as a zero reference mark, was generated by a coincidence of signals from counters in the incident-pion beam. There was a separate chronotron for each 90° ϕ sector of the neutron-counter array (see Fig. 3). The information on the polar and azimuthal angles of all the scattered particles detected and of the flight time ($\tau_n = 1, 2, 3, \cdots, 7$) of the detected neutron were buffer-stored in magnetic cores and transferred from there to magnetic tape.[9] The data on a tape were then analyzed in an IBM 709 computer by means of a kinematic fitting program.

B. Pion Beam

Figure 2 is a diagram of the beam-magnet layout. The internal target T_1 is placed in an almost field-free region of the Bevatron and is traversed by the internal proton beam. The quadrupole magnet Q_1 accepts particles scattered in a cone whose axis makes an angle of 32° with the internal beam direction. The height of Q_1 and of all the other magnets is adjusted so that the magnets are vertically centered about the median plane of the beam. The bending magnets M_1 and M_2 determined the momentum of the beam. A detailed description of the momentum spread of the beam, focusing properties of the magnets, and hot-wire calibration of the magnet system is given in reference 7. Table II gives a list of the magnets used.

Table II. Magnets used in the pion beam.

Magnet	Description
Q_1	8-in. doublet quadrupole
M_1	12 × 60-in. analyzing magnet
Q_2	8-in. doublet
Q_3	16-in. doublet
M_2	18 × 36-in. H-magnet
Q_4	8-in. triplet
Q_5	8-in. triplet

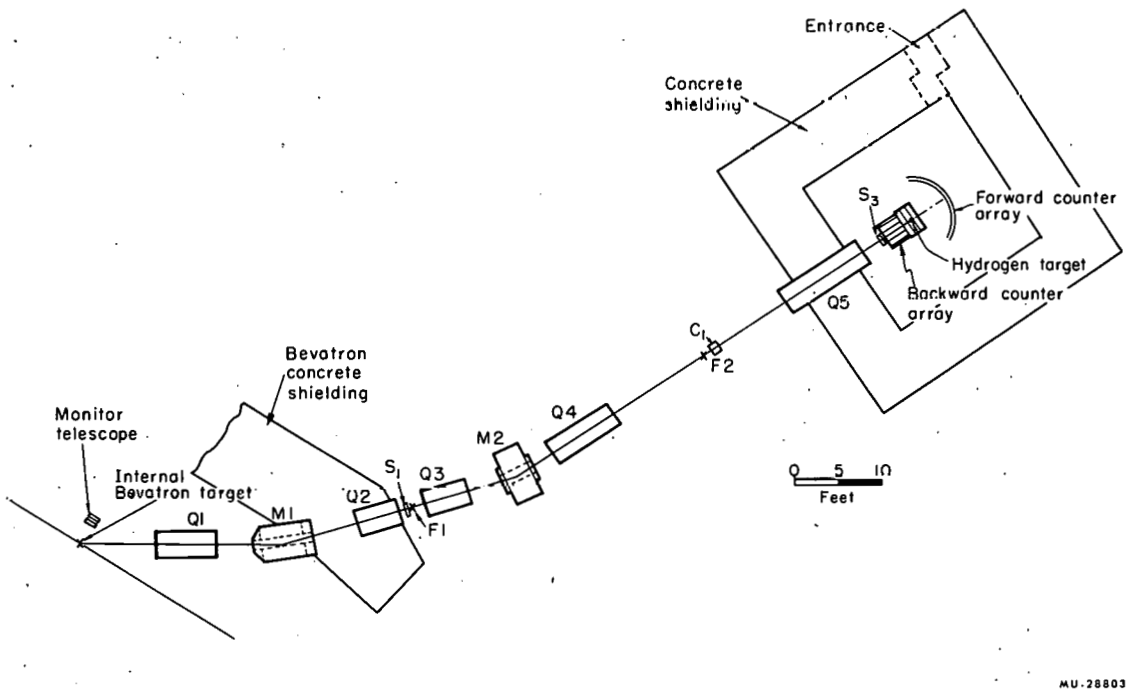

Fig. 2. Diagram of the magnet system and counter placement.

The placement of the beam counters S_1, C_1, S_3, and S_4 is also shown in Fig. 2. Counter S_1 was at the first focus and C_1 was at the second focus. Counters S_1 and S_3 were plastic scintillators (PS) connected by lucite light guides to RCA 6810A photomultipliers. Anticoincidence counter S_4 was a PS whose light output was funneled by a hollow electropolished aluminum light guide (trade name "Alzac") onto the face of an RCA 7046 photomultiplier. Counter C_1 was a cylindrical Cerenkov counter with axis along the beam. It was made of cyclohexene, with refractive index 1.47, and used a 6810A photomultiplier. This counter was designed to look at Cerenkov light that was totally internally reflected in the cyclohexene chamber. The β required to meet this condition was 0.94. For incident momenta of 1.25 and 1.75 BeV/c, protons have $\beta = 0.795$ and $\beta = 0.872$, respectively, whereas pions have $\beta \approx 1$ for both cases. The β's of deuterons and alpha particles are even smaller than those for protons. Thus, when a positive beam at either 1.25 or 1.75 BeV/c was run, the proton, deuteron, and alpha components could be discriminated against by a time-of-flight measurement with the additional requirement that the Cerenkov counter be made to contribute to a coincidence of $S_1C_1S_3$. Counter S_3 was upstream from the hydrogen target and S_4 was at the last focus, which was at the center of the forward counter array. It was used in anticoincidence with $S_1C_1S_3$ to define a particle scattered out of the beam.

C. Hydrogen Target and Counter Arrangement

The liquid hydrogen was contained in a hemispheric Mylar flask of 10 cm radius with the flat side facing the incident beam. The outer jacket had a Mylar window facing the beam and a 1/16-in. aluminum dome facing the counter array. Figure 3 shows how the counters were arranged with respect to the target and the incident beam. The forward counter array, (which will be referred to from now on as the "dish")consisted of 84 counters. These were designed to be approximately 25% efficient for counting neutrons in the energy range 5 to 60 MeV. They were made of 15-cm-thick plastic scintillator. Each block of scintillator was coupled by a hollow electropolished aluminum light guide to a photomultiplier. The blocks were trapezoidal prisms and were fitted together to form a section of spherical surface. A 1/8-in. -

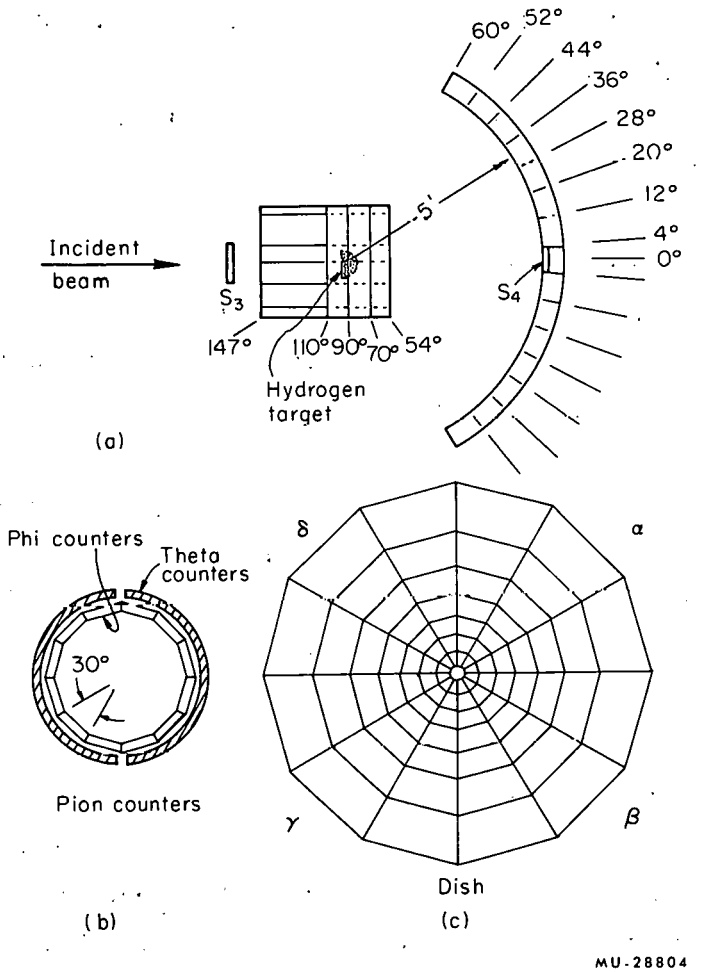

Fig. 3. Geometric arrangement of counters. The side view is shown in (a). Front views of the pion counters and the dish are shown separately in (b) and (c). (View as seen looking along the incident beam).

thick aluminum sheet was formed into a section of sphere and served as a faceplate for the counter assembly. Each block of scintillator was bolted to this plate. Provision was made for pulsed nanosecond light sources to be affixed to the face of each block.[10] Radial wedges of lead 1/4 in. thick were then fitted onto and attached to the plate, thus covering the entire array of 84 counters.

The lead was put in to convert decay gammas from π^0's produced in pion-nucleon collisions. The combined thickness of lead, aluminum, and scintillator was 1.64 radiation lengths, and gave a pair-conversion probability of 88% per incident photon. The lead served as an excellent discriminator against reactions in which two charged pions and one neutral pion were produced. Final states with $p+\pi^+ +\pi^0$ were also discriminated against because the large amount of absorber in the flight path of the low-energy protons stopped them before they could get into the forward counter array. The sphere geometry to which the array was fitted had a 160-cm radius with the hydrogen target at the center. The counters in the three inner rings had RCA 6810A photomultipliers. Those in the four outer rings had RCA 7046 photomultipliers. The angular interval subtended by each counter is given in Table III. The values listed are for a point-source target and for the 10-cm target actually used. The polar angle θ is the angle between the incident beam and the scattered particle. The azimuthal angle is called ϕ. The second group of counters, i.e., those surrounding the target, were for the detection of pions only. They were made of 1.0-cm-thick plastic scintillator, coupled by lucite light guides to 6810A photomultipliers. This group consisted of 12 ϕ counters arranged to fit like staves over a cylindrical frame enclosing the hydrogen target. In addition to these, there were six semicircular slat counters arranged in pairs to cover the forward circular surface of the cylinder (see Fig. 3). The angular intervals subtended by these counters are also given in Table III. For the limit of a point target, each of the 84 counters in the forward array and each of the 12 stave counters in the backward array had an azimuthal angular interval of 30 deg. The circular counters were used for a determination of θ only, and a single in

Table III. Angular intervals subtended by counters. All 84 counters in the dish and the counters in the backward array subtended azimuthal angular intervals of 30^{o} as defined by a point target. The physical size is $30^{o} + 2\delta\phi$.

Theta zone	Point-target limits (deg)		Physical limits (deg)		
	θ^{min}	θ^{max}	θ^{min}	θ^{max}	$\delta\phi$
1	4	12	2.2	14.1	13.8
2	12	20	9.9	23.3	4.7
3	20	28	17.7	30.5	2.8
4	28	36	25.5	38.7	2.0
5	36	44	33.4	46.8	1.6
6	44	52	41.3	54.9	1.4
7	52	60	49.2	62.9	1.2
8	54.5	70	57.8	81.4	5.3
9	70	90	58.1	102.2	5.3
10	90	110.5	77.8	122.8	5.3
11	110.5	147.5	98.6	155.1	5.3

one of the θ counters had to be accompanied by a signal in one of the ϕ counters in order to be correlated with a particle traversing these counters. A 1/4-in. thickness of lead was inserted between this second group and the target. A concrete blockhouse with walls and ceiling 8 ft thick was built around the counter-target assembly to provide shielding against the neutron background coming from the Bevatron. The last quadrupole in the magnet system was buried in the entrance aperture of the blockhouse. For the second group of counters (those counting pions only) the probability for conversion of a γ ray into a pair (e^-e^+) was 81%.

D. Electronics

1. Information Storage

The complete block diagram for the electronics is given in Fig. 4. The output from each counter is put into a tunnel diode discriminator circuit in order to get good timing on the pulses.[11] Two sets of signals are taken from these discriminators. One set consists of individual outputs from all the counters. These signals go to the pion and neutron coincidence-discriminator (CD) units. If the timing requirements have been met, the CD units cause information to be stored in appropriate locations in the buffer storage (magnetic-core storage)(see the following section). The other set consists of a mixture of the signals into the counters in dish sectors Aα, Bα, Aβ, Bβ, Aγ, Bγ, and Aδ, βδ (see Fig. 3). These are further combined to give just α, β, γ, and δ. Each of these lines is then fed into a gating circuit (n gate). If the gate is open, the signal that gets through is then timed in the chronotron, and the information from the chronotron is sent to the storage unit. The CD units, buffer storage, and transfer-to-magnetic-tape circuitry are fully described in reference 12.

2. Overall Trigger System

A simplified diagram of the triggering system is given in Fig. 5. In essence, the system makes the twofold requirement that a particle be scattered out of the beam and that a slow particle be detected in the forward counter array (dish) before information can be stored in the magnetic-core storage units. When a particle is scattered out of the beam,

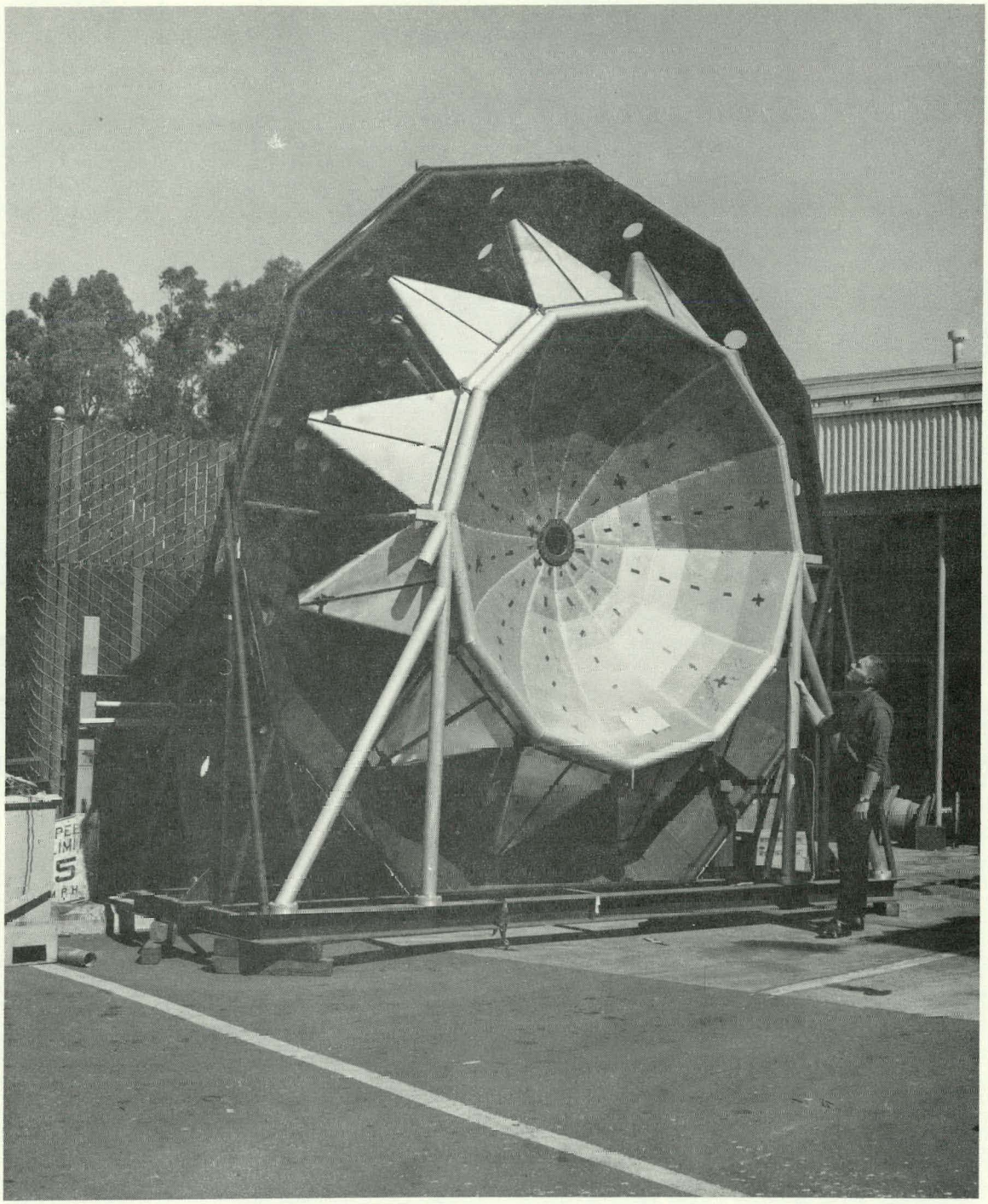

ZN-3412

Fig. 4. Photograph of counter dish.

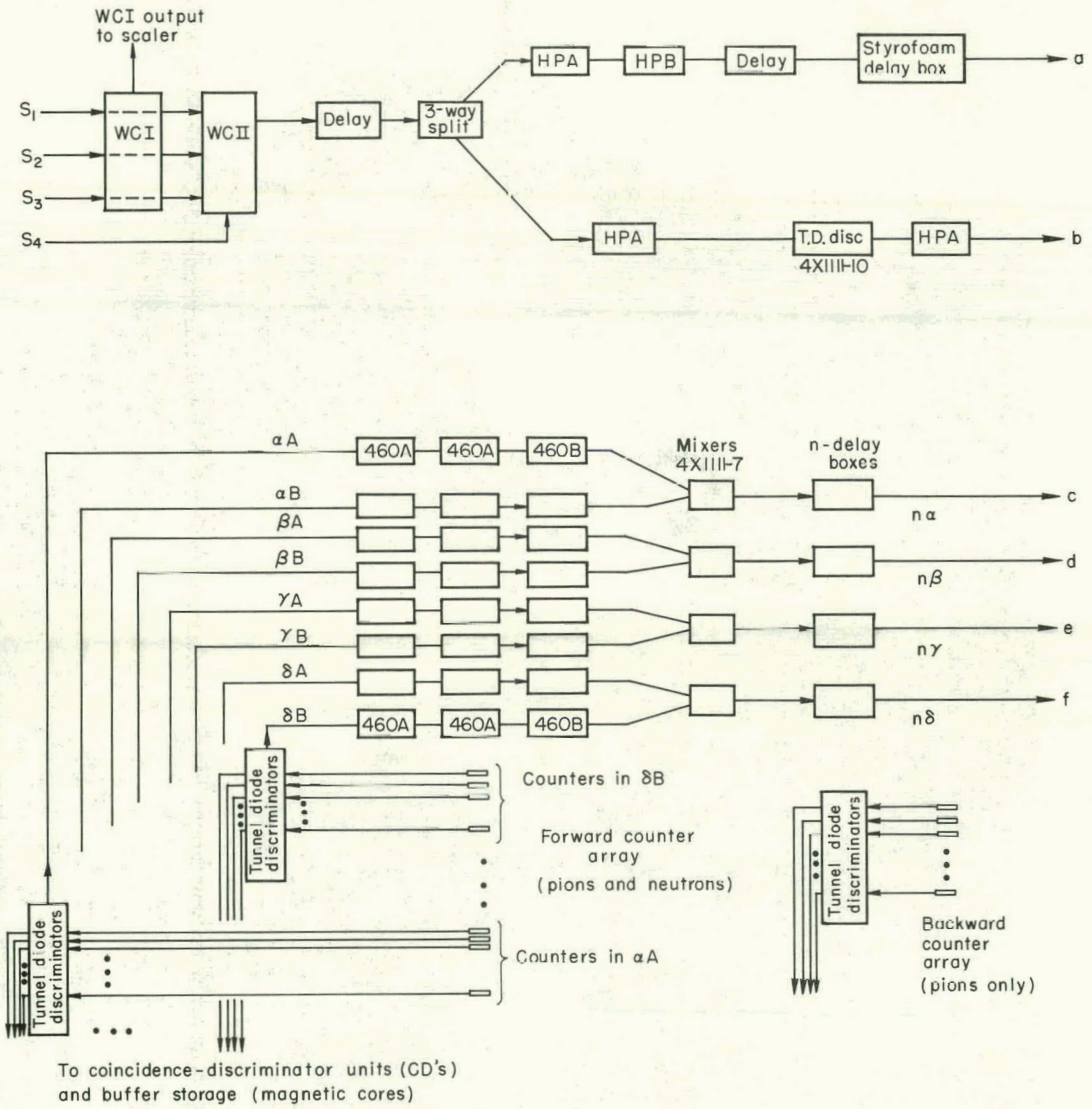

Fig. 5a. Block diagram of electronics (Part 1).

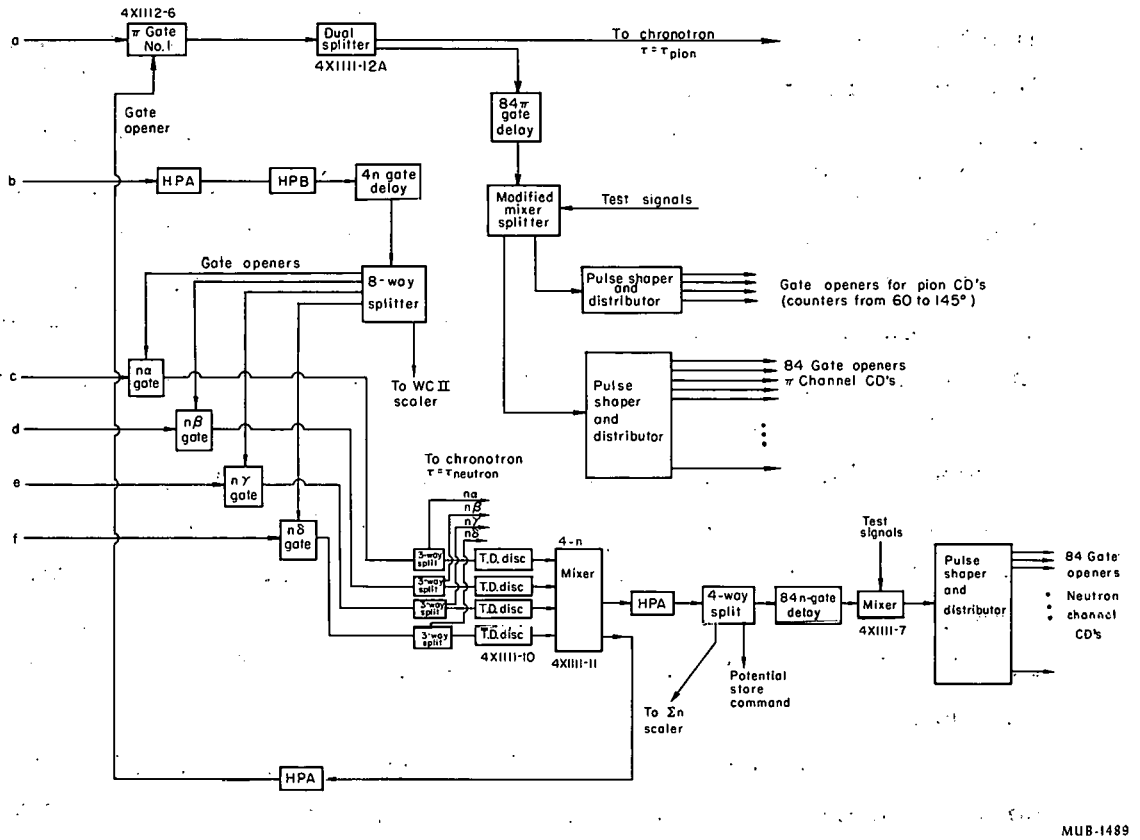

Fig. 5b. Block diagram of electronics (Part 2).

the signal ($S_1 C_1 S_3 \bar{S}_4$), which is the output of the fast coincidence WC II, is split into two branches. The signal in one of the branches is used to open four neutron gates, one for each of the sectors α, β, γ, and δ of the dish. These gates stay open for approx 50 nsec and the front edge of the gate occurs approx τ_n^{min} nsec after the arrival of an incident-beam particle at the hydrogen target, where τ_n^{min} is the flight time of the highest-energy neutron accepted by the system, and $\tau_n^{max} \approx \tau_n^{min} + 50$ nsec corresponds to the lowest energy. (See Table I for the actual chronotron-time boundaries.) The procedure for setting the timing is given in a later section. If a signal comes along one of the neutron lines (n lines) in the interval $\tau_n^{min} \leq \tau_n \leq \tau_n^{max}$, it gets through the n gate. It is then split and goes along one of the branches to the time-of-flight coincidence circuitry (chronotron) and to the gate generator that allows neutron information to go through the CD units into the magnetic cores. Another branch of the signal is used to open the π gate. If this π gate is opened, the signal $S_1 C_1 S_3 \bar{S}_4$ can get through to initiate storage of pion information in the cores (by gating on the pion CD units.) It also provides a zero reference time for the chronotron.

As shown in Fig. 5, the signals from the incident-beam counters were fed into two fast-coincidence circuits WCI and WCII. The WCI output ($S_1 C_1 S_3$) gave the flux of particles incident on the target. Since the accuracy of the scattering-cross-section determination was dependent, among other things, on the accuracy of the incident-flux determination, the WCI circuit was very carefully tested at the beginning of each data run. The ratio WCII/WCI was also carefully monitored, since it had to remain constant for a fixed amount of scattering material in the target and for a fixed incident-particle momentum.

3. Timing

a. Beam counters

Since the positively charged beam incident on the hydrogen target was composed primarily of pions, protons, deuterons, and alpha particles (see reference 7 for lepton contamination), it was necessary to make an electronic selection of those that were pions. To do this, we

took a curve of S_1S_3/monitor vs S_3 delay, using the monitor counter telescope (shown in Fig. 3) as a flux standard for the S_1S_3 rate. Using the known S_1S_3 separation distance and the values of β for the various particles, we determined which of the peaks on this curve corresponded to pions and set the S_3 delay accordingly. The Cerenkov counter C_1 was then included and the $S_1C_1S_3$/monitor was taken vs C_1 delay. As explained earlier, the β selection of C_1 was a guarantee that we would count only the pions of the particles mentioned above. The operating voltages for each counter were determined by taking curves of the coincidence count rate vs voltage and setting the operating voltage in the plateau region of the curve. The approximate timing on S_4 was determined by putting it in coincidence with S_1C_1 and taking a curve of $S_1C_1S_4$/monitor vs S_4 delay. Then it was put in anticoincidence with $S_1C_1S_3$, and the appropriate final delay and high-voltage settings were determined. The signal $S_1C_1S_3\bar{S}_4$ was of central importance to the experiment because, by opening the neutron gates (n gates in Fig. 5), it determined how often the apparatus would be allowed to search for slow-neutron events. Appropriate care was taken to determine the voltage at which S_4 should operate. It was necessary that it should reliably count all pions from the incident beam that traversed it so that the number of false triggers be kept at a minimum. It was also necessary to keep the noise level low enough so that real scatterings (no particle crossing S_4) did generate triggers.

b. Forward array (Dish) counters

The plastic scintillator in these counters consisted of approx 97% polystyrene (CH), approx 3% terphenyl, and 0.03% tetraphenyl butadiene. In order to measure and adjust the timing of these counters, it was first necessary to determine the voltage at which each of them should operate, so they would all have approximately the same threshold, i.e., so all the counters would reliably detect the light output from 3- to 4-MeV protons. To equalize the thresholds, a Na^{22} source of known strength was placed against the aluminum face plate near the center of each counter. It was required that the net counts/sec coming from the

1.28-MeV γ rays from the Na^{22} be approximately equal for all counters. The bias voltages on the tunnel-diode discriminators were all set to accept signals of 180±20 mV. This setting was made to insure stable operation of the tunnel diodes. The signal output from the counters was in all cases large enough to fire the discriminators reliably. For each of the seven counter sizes (one for each θ ring), we measured the Na^{22} count rate for various positions of the source across the face of the counter. There was no noticeable variation, within statistics, so that no special care had to be taken in positioning the Na^{22} source for these measurements. The high voltage on each counter was varied until the desired net count rate was obtained as nearly as possible for the lowest "source out" (noise) rate. In those cases in which the desired net counts could not be obtained without excessive noise, the phototubes were replaced until the desired net rate could be gotten with a low noise level.

Timing measurements were made on signals generated by a pulsed light source screwed into a hole in the face plate at the center of each counter. One high-voltage trigger, connecting cable and light bulb, was used for all the counters in the dish. The light pulser operated at a fixed frequency (number of light pulses per sec). The pulses from a tube in one of the sectors (α, β, γ, or δ) were counted after they came through the corresponding neutron gate, and the count rate was measured (on a scalar) as a function of the delay in the neutron line (n-delay box, see Fig. 5).

The high voltages on all the other phototubes in the sector (α, β, γ, or δ) were turned off. Thus at the time of measurement, the only source of signals along the neutron line was the counter being investigated. A typical delay curve was Gaussian with a full width at half maximum of approx 3 nsec. The center of such a curve was measurable to within approx 0.2 nsec. A pulsed light source (operating from the same trigger used for the counter being measured) was used to generate the WCII signal that opened the n gate. After such curves had been taken for all the counters in a given sector, the cable lengths between the counters and the tunnel-diode discriminators (see Fig. 4.) were adjusted so

that the arrival time of pulser signals from all counters in a sector would be the same at the neutron gate and also at the chronotron of the sector in question. The timing was done for all four sectors. The light-pulser signals were also used to measure the arrival time of signals at the CD units. These CD units were circuits that, when gated on from the "super splitters" by an overall trigger, accepted signals from the counters and shaped them as needed for registering them in the magnetic-core storage. No information could get through the CD units and into the magnetic cores unless these CD's were gated on. Signals from each of the dish counters were fed through CD's into both a neutron and a pion buffer unit. Signals from the counters between 60° and 147° were fed into pion buffers only. As shown in Fig. 5, it was the WCII signal (which got through π gate No. 1) that gated on the CD units. These, in turn, permitted storage of pion information in the magnetic cores. The storage-permit signals for neutron information came from the signal line coming out of the mixer that combined the $n\alpha$, $n\beta$, $n\gamma$, and $n\delta$ lines. The timing measurements were all carried out with a trigger and gating system as similar as possible to the ones used in actual data runs.

c. Gates and Chronotron

To do the timing on the gates, we used fast particles ($\beta \approx 1$) produced in π-p scattering. Under normal operating conditions, the delay in the n lines would be arranged to make the signals from the highest-energy neutrons we wished to study (τ_1 neutrons) fall in the center of time bin No. 1 of the chronotron, with lower-energy particles going into higher-numbered time bins. Since there was no a priori way of selecting neutrons (produced in π-p scattering) of a given energy and flight time, the timing had to be done with particles of known flight time. This was accomplished by inserting in the neutron lines an amount of delay equal to the difference in flight time between a particle with $\beta \sim 1$ and a τ_1 neutron. (The flight path in question was the 160-cm distance between the center of the hydrogen counter and the face of the dish counters). With this technique, by making cable changes where necessary in other lines, delay curves were taken to time and adjust the various

gates shown in Fig. 5. The zero reference time for the chronotron and the widths of each chronotron time bin were also set in this way. Since the time-bin widths would be correlated with the spread in neutron energy in a given bin, a procedure was set up to allow periodic checks of these widths with consequent adjustment, if necessary. This would assure us of having a neutron resolution (associated with each time bin) that stayed quite constant throughout the experiment. Even though particles with $\beta \sim 1$ were used in the testing, we were able to simulate a time-of-flight spectrum simply by changing the amount of delay in the neutron lines. In this way, we could record the number of counts registered in each time bin for a given delay, and by systematically varying the delay and making a count tally for that delay value, we could make a distribution of counts vs delay for each time bin. These distributions were made for all four chronotrons. The measured widths of each time bin were then used as guides to indicate how much adjustment was needed to obtain the settings in Table I. After adjustments were made, the curves were rerun to make sure that the widths were as desired. For example, $\Delta\tau_{1\alpha}$ was set equal to $\Delta\tau_{1\beta,\,\gamma,\,\delta\,\cdots} = 2.8$ nsec, etc. Typical distribution curves are shown in Fig. 6. The width of a time bin is measured between the points where its distribution intersects those of adjacent bins. The chronotron also had end bins, so that all counts arising from pulses coming outside(later than)bin No. 7 fell into end bin No. 00, and those coming earlier than bin No. 1 counts fell into end bin No. 0. This made it possible to measure the widths of bins No. 1 and No. 7. Included in this timing work was a precise determination of how much delay should be in the neutron lines in order that $\beta \sim 1$ particles fall at the center of time bin No. 1. The shift to neutrons of a given flight time was then completely determined. The time-bin widths, measured periodically throughout the course of the experiment, did not vary by more than 0.3 to 0.4 nsec.

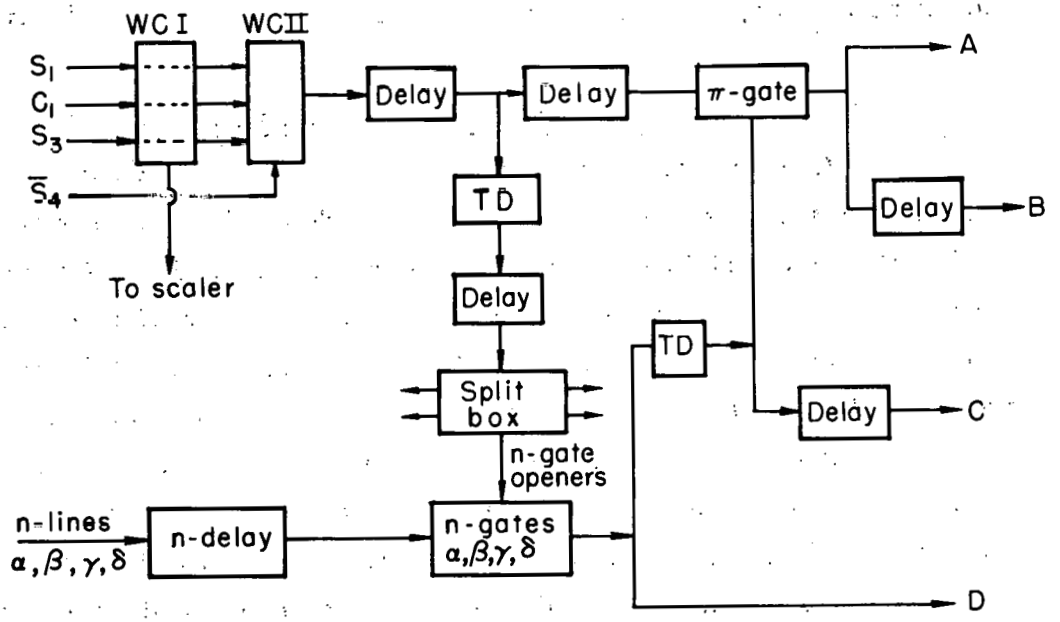

Fig. 6. Simplified diagram of overall trigger system. From point A, the signal goes to the chronotron, where is provides the zero reference time τ_0 corresponding to the flight time of a pion, with $\beta=1$, between target and dish. From B, the signal goes to gate-generator units which provide pulses that gate on the pion CD units. From C, the neutron CD units are gated on. From D, the signal goes to the chronotron to give the neutron timing τ_n compared with the reference signal τ_0.

d. Counters between 60° and 147°

The timing of these counters was done at the junctions where their signals went into the pion CD units. It was required that their signals arrive simultaneously with respect to the front edge of the gate and that they be reliably within the gate. Curves of high voltage vs count rate (plateau curves) were taken with beam-derived particles.

E. Determination of Neutron Counting Efficiency

Our measurement of the detection efficiency of our system for neutrons in the range 4 to 76 MeV is described here only briefly. A detailed account is given in reference 13. A 205-MeV neutron beam, produced by stripping deuterons accelerated in the 184-inch Lawrence Radiation Laboratory synchrocyclotron, was scattered from a hydrogen target. The protons were detected in a range telescope and the conjugate elastically scattered neutrons went into a counter identical with one of the counters in the dish. The distance to the neutron counter was 160 cm, and the gating was identical with that used in the data runs except that the WCII signal was replaced in this case by a stopped proton signal. A run consisted of measuring the number of counts in each chronotron time bin for a given setting of proton-telescope and neutron-counter angle. The neutron efficiency after subtractions for background have been made is the ratio of neutron counts to proton counts. The neutron energy for such a setting was known, from proton range, kinematics, and proton telescope geometry, to within 1.2 MeV for neutrons of kinetic energy 6.8 MeV and to within 5 MeV at a kinetic energy of 46 MeV. The results for a counter identical with those in θ zone 5 of the dish are shown in Table IV. The overall efficiency ϵ is the efficiency for the sum of all time bins, i.e., bin No. 0 + bin No. 1 + $\cdots$ + bin No. 7 + bin No. 00. Eta is the efficiency for bins 1 through 7 and E_n is the kinetic energy of the incident neutron. Measurements at several values of E_n were made on zone No. 2 and zone No. 7 counters. The results for efficiency vs E_n were equal, within statistics, with those for zone 5.

Table IV. Neutron counting efficiency in θ zone 5; ϵ is the efficiency summed over time bins 0 through 00; η is the efficiency summed over bins 1 through 7; E_n is the kinetic energy of the incident neutron.

E_n (MeV)	ϵ (%)	η (%)
4.4	2.1	2.1
6.8	24.2	14.4
9.8	31.4	28.2
13.3	29.9	28.8
17.2	31.6	30.9
23.9	29.1	28.6
28.8	30.0	29.9
34.2	29.2	28.9
40.0	26.8	26.2
45.9	27.3	25.8
58.7	23.7	18.9
62.0	25.0	12.8
75.8	19.2	4.4

For purposes of calculation, it was assumed that all counter sizes (θ zones 1 through 7) in the dish had equal efficiencies for neutron detection. Curves of neutron-detection efficiency vs neutron kinetic energy are given for each time bin in Fig. 7. A curve of the total efficiency ϵ is given in Fig. 8.

F. Experimental Procedure

A data run consisted of a measurement of the scattering $\pi^+ + p \rightarrow \pi^+ + \pi^+ + n$ under the following four conditions:

1. The hydrogen target full, the delays set for looking at the low-energy neutron spectrum.

2. The target emptied of hydrogen, the delays as in 1. This measured the non-hydrogen-derived scattering background at normal delay.

3. The target full, but delay added to the neutron lines. Enough delay was added so that no particles from the scattering that triggered the electronics could get through the neutron gates. A real particle from the scattering would have had to have $\beta > 1$ in order to get through the neutron gate. Thus, purely random background from cosmic rays, induced activity, and decays in the dish, etc., which would contribute to the full normal condition were measured by using this abnormal delay condition.

4. The same delay condition as 3, but target emptied of hydrogen.

The information from the runs was recorded on magnetic tape. Generally, one magnetic tape was used per run. The scaler registering the number of Bevatron pulses was reset to zero at the beginning of each run. A series of "fixed data" switches were set to record on tape which of the four conditions (target full, delays normal, target empty, delays normal, etc.) was being measured. The Bevatron pulse number for each set of events was also recorded on the tape. There were generally about fifty scattering events stored per Bevatron pulse. Because of core-storage limitations, the information in the cores was transferred to magnetic tape after ten events had been stored.

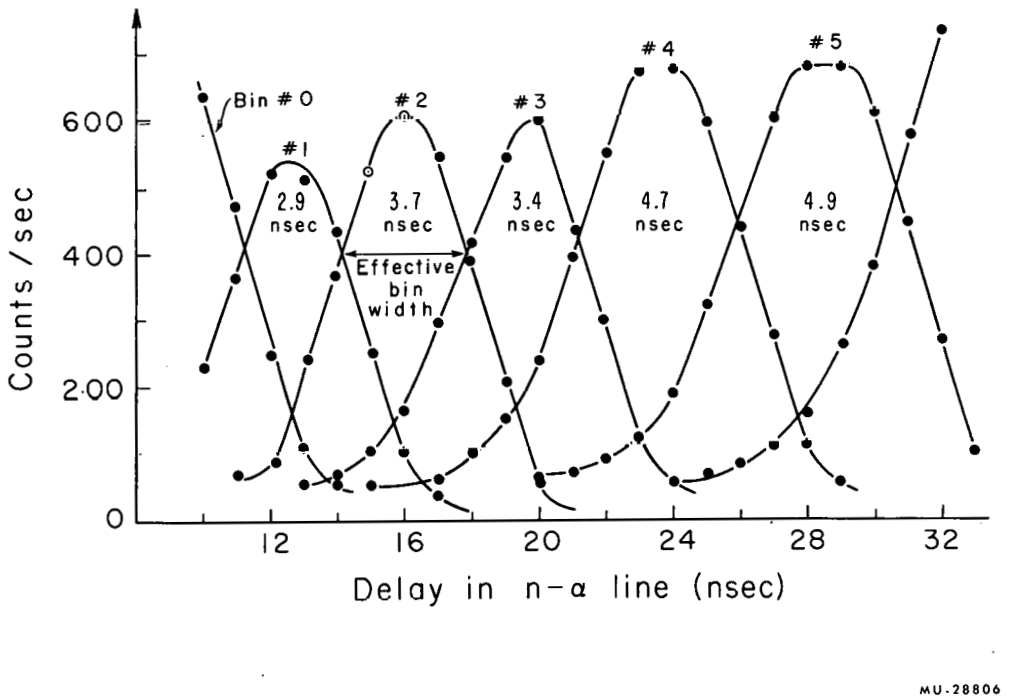

Fig. 7. Measurement of chronotron time-bin widths. Only bins 1 through 5 are shown. The data shown here are for dish quadrant α. Each quadrant of the dish had a separate chronotron.

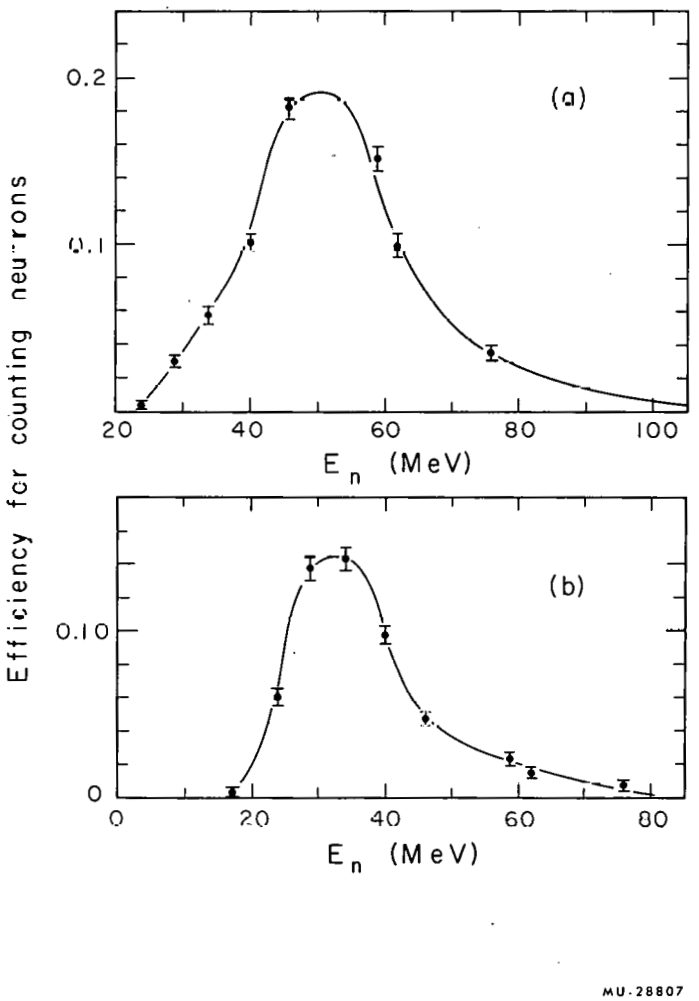

Fig. 8a, b. Neutron counting efficiency η as a function of incident neutron kinetic energy E_n.

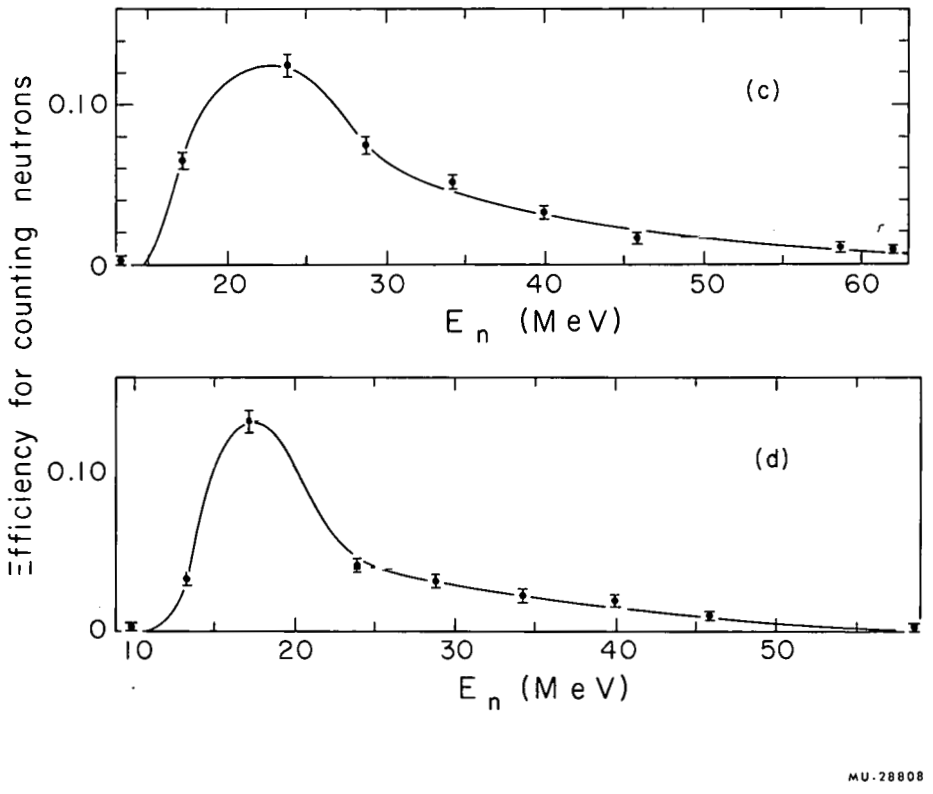

Fig. 8c,d. Neutron counting efficiency η as a function of incident neutron kinetic energy E_n.

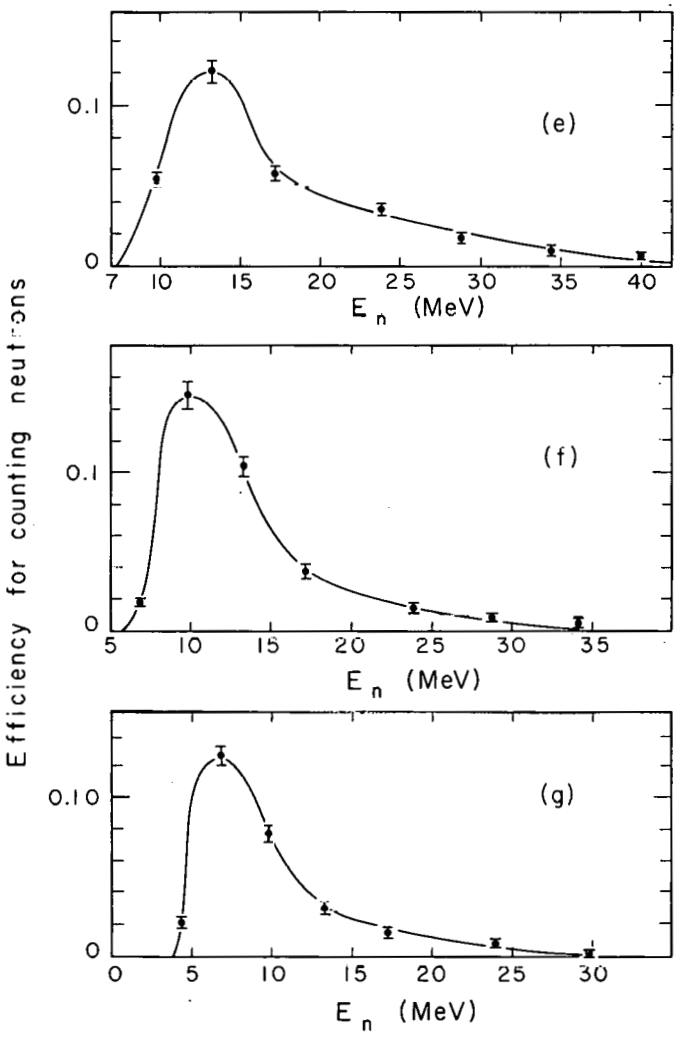

Fig. 8e,f,g. Neutron counting efficiency η as a function of incident neutron kinetic energy E_n, for (e) time bin 5, (f) time bin 6, (g) time bin 7.

During this transfer interval, "inhibit" signals gated off the incident-flux scalers and the data-storage electronics. A master gate, from a scaler gater and beam monitor, gated off the scalers, etc. between Bevatron pulses.

During each data run, the following information was registered on scalers:

a. WCI: incident flux;

b. WCII: the number of particles scattered out of the incident beam at an angle greater than 4^{o};

c. N_{α}, N_{β}, N_{γ}, and N_{δ}: the number of scattered particles (detected by each ϕ sector of the dish) that gave rise to signals satisfying the timing requirement for neutrons to get through the n gates;

d. N_{τ_0}, N_{τ_1}, $\cdots$, $N_{\tau_{00}}$: the breakdown of c for one of the sectors into number per time bin. During a run, the output of only one of the chronotrons could be registered on scalers in this way;

e. Monitor (Mon): the number of counts registered in the monitor telescope;

f. N_D: the total number of pulses from the dish;

g. N_{BeV}: the number of times the Bevatron pulsed during the run; and

h. $\Sigma n = N_{\alpha} + N_{\beta} + N_{\gamma} + N_{\delta}$.

The ratio WCI/Mon served as a sensitive check on how the internal beam was steered with respect to our internal target. The position of the internal target was varied to make WCI/Mon a maximum. Before each data run, curves were taken of the variation in WCI and WCII as a function of the current in the first bending magnet (M_1) in order to obtain a setting for M_1 that simultaneously maximized WCI/Mon and minimized WCII/WCI.[7]

Since the scattered neutrons had, from symmetry considerations, to be uniformly distributed in ϕ, the N_{α}, N_{β}, N_{γ}, and N_{δ} helped to show (on those rare occasions when the scalers were working) whether or not this condition was being satisfied, and served as an aid in locating malfunctioning components when a nonuniformity was observed

that lay outside statistical fluctuation. The Σn scaler served as a check on the requirement that, if properly timed signals got through to the tunnel-diode discriminators in the four neutron lines, there would always be a corresponding "potential-store command" and a gating open of the neutron CD units (see Fig. 4). Since the output of only one of the chronotrons could be registered on scalers during a run, a series of runs was required to show whether or not (the number of counts)/(time bin in chronotron α) agreed with that in β, etc. when normalized for incident flux. This test could be made quickly--compared with the time required for comparison--by using the results from computer-analyzed magnetic tapes.

A visual display of small lamps so arranged as to simulate the corresponding detectors showed the location of all particles detected for the first scattering-event stored during a Bevatron pulse. Fast and slow particles were separately displayed, and the time-bin signature of the slow particles was shown for all four chronotrons. The information displayed could be read from the cores, from the magnetic tape, or from a core-tape comparison. A continual read-write test was thus available. Also, spot checks could be made of the particle multiplicity and angular distributions. Statistics were limited, since only 10 events per minute were displayed. (The Bevatron pulses once every 6 seconds). However, if one of the counters in the dish became noisy, this could be seen in a matter of minutes. Also, as shown in the block diagram, test signals were available that simultaneously activated all the CD units, and the visual display could be used to determine which units were not working properly. The information transfer from cores to magnetic tape could also be tested this way. The test routines are described by Baker et al.[14]

Periodic checks were made on the coincidence circuits WCI and WCII and their associated scalers, by using pulses from a mercury switch pulser. The timing of gates and of every tube in the detector system was measured many times during the course of the experiment, and checks were made almost every day on a few randomly selected counters. The sensitivity measurement of the dish counters, using Na^{22},

was done weekly during the down time of the Bevatron. Where it was necessary to change high voltage on the phototubes, the timing was redone and adjustments made wherever necessary.

A data run was made by using an incident proton beam of 830 MeV/c to measure the total p-p cross section and compare it with a previously measured value.[15] This was done before the lead covering was placed on the dish. The gate timing was adjusted to correspond to the scattered proton energies, and detection of the forward proton only was required. The results of this measurement were in excellent agreement with the known value of the cross section. With the exception of the slight shift in timing, all other features of the apparatus (trigger system, chronotron, data storage, etc.) were used exactly as they would be to investigate the reaction $\pi + p \rightarrow \pi + \pi + n$. The visual display for those scatterings (p-p) in which both particles hit the dish showed in all cases a 180° ϕ separation and the correct θ separation.

As mentioned earlier, the reaction $\pi^{+} + p \rightarrow \pi^{+} + \pi^{+} + n$ (reported in this paper) was not the only one studied. We also measured the low-energy neutron cross sections for the reactions $\pi^{-} + p \rightarrow \pi^{-} + \pi^{+} + n$ and $p + p \rightarrow p + \pi^{+} + n$. To insure constancy in the behavior of the apparatus, we ran each of these reactions only a few days at a time, switching successively from one to another. We checked to see that the total cross sections and distributions in energy and angle that we measured were the same--within statistics--from measurement to measurement for the same reaction.

III. RESULTS AND ANALYSIS

A. Preparation of Data

The data on the magnetic tapes were analyzed by a kinematic fitting program on an IBM 709 computer. First, events were sorted on the basis of how many particles had been detected in the neutron circuitry and how many in the pion circuitry. Thus, there were event categories 1 neutron, 1 pion; 1n, 2π; 1n, 3π; etc. The same was done for two-neutron events, i.e. 2n, 1π; 2n, 2π; etc., and for 3n, 1π; 3n, 2π; $\cdots$. The only events that were tested for kinematic fit were those with a 1n, 2π signature. A complete description of the data-handling process and of the search program used to test each 1n, 2π event for a kinematic fit is given in reference 16. The final form of the data for a given reaction at one value of incident momentum was put on a master tape. On this tape (master packed) were listed all 1n, 2π processed by the electronics during the data runs for the reaction in question. For those events for which momentum and energy conservation could be satisfied, the variables of the final set used in the program were listed. We refer to them as "search values." This master tape was then suitable for use as a data-input tape on an IBM 709 or 7090 computer, and all cross sections, distributions, etc. could be determined from these data by appropriate programming for the computer.

B. Method of Analysis

As we have said in the introduction, our primary goal was to measure the cross section for the scattering of low-energy neutrons per unit range of p^2 and ω^2, i.e., $\partial^2\sigma/\partial p^2 \partial \omega^2$. The variables p^2 and ω^2 are given as functions of the laboratory-system kinetic energy T_{2L} and the lab scattering angle θ_{2L} of the neutron by $p^2 = 2M_n T_{2L}$ and $\omega^2 = (\omega_{1L} + M_p - M_n - T_{2L})^2 - (q_{1L}^2 + p_{2L}^2 - 2q_{1L}p_{2L}\cos\theta_{2L})$, where M_p and M_n are the proton and neutron masses, respectively; q_{1L} and ω_{1L} are momentum and energy of the incident pion, $\omega_{1L}^2 = q_{1L}^2 + \mu^2$, and p_{2L} is the momentum of the scattered neutron, $(M_n + T_{2L})^2 = p_{2L}^2 + M^2$. All variables are referred to the laboratory frame of reference. Before

explaining the method used for assigning a value of p^2 and ω^2 to each event that satisfied kinematics, we would like to clarify, qualitatively, the meaning of the phrase "a kinematic fit" as used in this paper. Referring back to Table III, we see that the counters had angular intervals of approx 10^o in θ and approx 30^o in ϕ. The neutron energy range corresponding to each time bin (see Fig. 7) was quite large. The search program was given the angular intervals for the counters in which the particles were detected and the energy interval for the time bin in which the neutron pulse was recorded. The program then made a systematic search through the ranges of these variables, many times if necessary, to see if there existed a set that satisfied conservation of energy and momentum. If such a consistent set was found, no further searching was done to look for other sets. Thus the search values assigned to each good event were accurate only to within the angular limits defined by the counters. To obtain accuracy in accord with the limits placed on us by our resolution in angle and energy, the good-fit events were sorted on the basis of their neutron θ-zone and time-bin signatures. At a fixed incident momentum, T_{2L} determined p^2, and T_{2L} and $\cos\theta_{2L}$ determined ω^2. The mean value of p^2 had to be obtained for each time bin, and the mean value of ω^2 had to be determined for each of the 49 pairs $\{\tau_j, \theta\text{-zone}_k\}$. Calling $\eta_j(T_{2L})$ the detection efficiency of our system for neutrons of kinetic energy T_{2L} for the jth time bin, the mean value of p^2 for that time bin is

$$\left\langle p_j^2 \right\rangle = \frac{\int (2M_n T_{2L})\, \eta_i(T_{2L})\, dT_{2L}}{\int \eta_j(T_{2L})\, dT_{2L}}, \qquad \text{(III-1)}$$

where the integration is carried out numerically over the efficiency curves $\eta_j(T_{2L})$. The rms spread $\delta p_j^2 = [\langle p_j^2 \rangle^2 - \langle (p_j^2)^2 \rangle]^{1/2}$ is gotten by evaluating $\langle (p_j^2)^2 \rangle$ from the same set of functions $\eta_j(T_{2L})$.

If the detection efficiency $\zeta_k(\cos\theta_{2L})$ is known for each of the seven θ zones of the dish, then for fixed j and k we can find $\langle \omega^2_{jk} \rangle$ from the equation

$$\left\langle \omega^2_{jk} \right\rangle = \frac{\iint \omega^2(T_{2L}, \cos\theta_{2L})\eta_j(T_{2L})\zeta_k(\cos\theta_{2L})dT_{2L}\,d(\cos\theta_{2L})}{\iint \eta_j(T_{2L})\,\zeta_k(\cos\theta_{2L})dT_{2L}\,d(\cos\theta_{2L})} . \quad \text{(III-2)}$$

As mentioned earlier, the sensitivity of counters in each of the θ zones of the dish was measured as a function of position of the Na^{22} source on the face of the counters. The response was uniform across the face. Thus, ζ_k could, to first approximation, be set equal to unity for each θ interval. However, as shown in Table III the limits on θ_{2L} for a given θ zone exceed those given for a point target. To take account of this smearing in angular resolution, the functions $\zeta_k(\cos\theta_{2L})$ used in the integration were trapezoids of height unity, of width 8° at half-height, and of width $\theta_{max}-\theta_{min}$ at the base, with θ_{max} and θ_{min} as given in Table III for our target. The mean values $\langle p^2 \rangle$ and the rms errors δp^2 as well as the corresponding $\langle T_{2L} \rangle$, δT_{2L} are given in Table V.

In Figs. 9 and 10 we have shown the region of (ω^2, p^2) phase space available at incident pion momenta of 1.25 and 1.75 BeV/c when neutron detection is restricted to the interval $60^\circ > \theta_{2L} > 4^\circ$, $6.5\,\mu^2 \geq p^2 \geq 0.5\,\mu^2$. The mean values $\langle p_j^2 \rangle \langle \omega^2_{jk} \rangle$ at which the cross sections $\partial^2\sigma/\partial p^2 \partial \omega^2$ were measured are shown in these figures.

To evaluate the cross sections $\dfrac{\partial^2 \sigma_{jk}}{\partial p^2 \partial \omega^2}$ for each time bin (j = 1, 7) and each θ interval (k = 1, 7), the effective areas $(\partial p^2 \partial \omega^2)_{jk}$ must be calculated. If p^2 and ω^2 are treated as independent variables, we can relate $dp^2 d\omega^2$ to $dT_{2L}\,d(\cos\theta_{2L})$ by the Jacobian for the transformation. This gives us the equation

Table V. Mean values of p^2/μ^2 and T_{2L} for the seven time-of-flight intervals, and the corresponding rms errors.

Time bin	$T_{2L} \pm \delta T_{2L}$ (MeV)	$p^2/\mu^2 \pm \delta p^2/\mu^2$
1	54±14	5.15 ± 1.32
2	38±12	3.65 ± 1.12
3	29±10	2.85 ± 0.96
4	23±8	2.25 ± 0.81
5	18± 7	1.70 ± 0.68
6	13± 5	1.30 ± 0.53
7	10± 5	0.98 ± 0.47

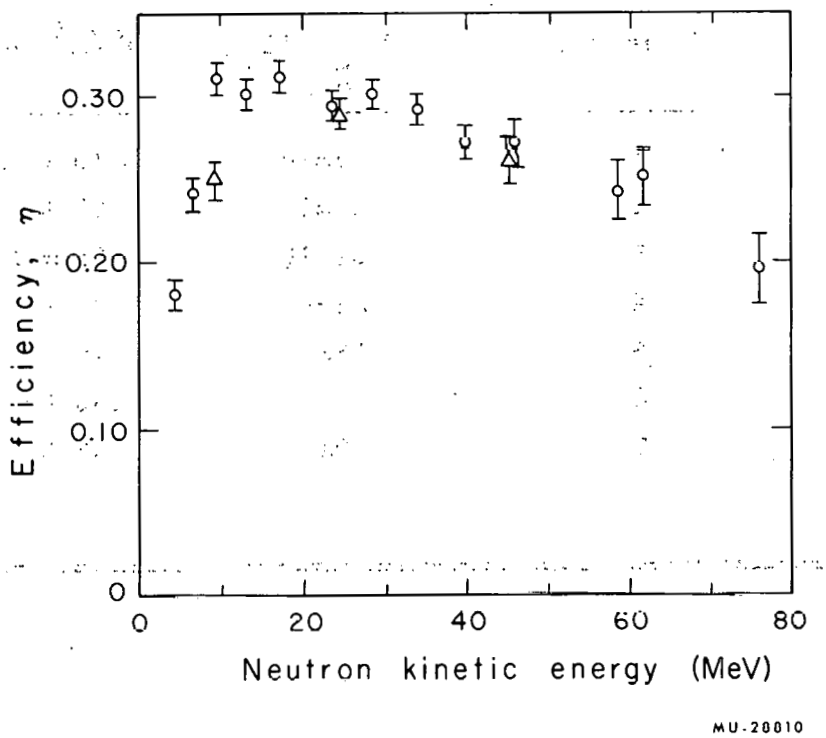

Fig. 9. Total efficiency for detecting neutrons.
O Theta zone No. 5.
Δ Theta zone No. 2.

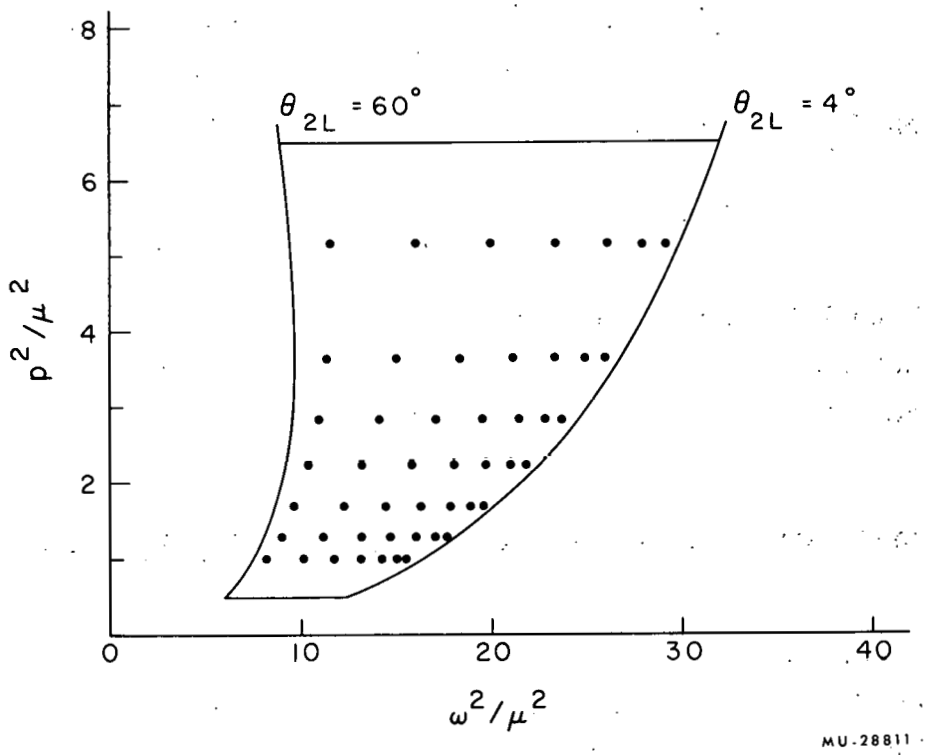

Fig. 10. The region of $(\omega^2, \mathbf{p}^2)$ phase space investigated in this experiment. The points $(\overline{\omega^2}/\mu^2, \overline{p^2}/\mu^2)_{jk}$ at which the cross sections $\partial^2\sigma/(\partial p^2/\mu^2\ \partial\omega^2/\mu^2)$ were evaluated are shown by ●.

$$dp^2\, d\omega^2 = \begin{vmatrix} \frac{\partial p^2}{\partial T_{2L}} & \frac{\partial p^2}{\partial(\cos\theta_{2L})} \\ \frac{\partial \omega^2}{\partial T_{2L}} & \frac{\partial \omega^2}{\partial(\cos\theta_{2L})} \end{vmatrix} dT_{2L}\, d(\cos\theta_{2L}). \qquad \text{(III-3)}$$

Since $p^2 = 2M_n T_{2L}$, $\partial p^2/\partial(\cos\theta_{2L}) = 0$, so that

$$dp^2 d\omega^2 = \frac{\partial p^2}{\partial T_{2L}} \quad \frac{\partial \omega^2}{\partial(\cos\theta_{2L})} \times dT_{2L} d(\cos\theta_{2L}).$$

Evaluating the Jacobian and using $p_{2L} = (2M_n T_{2L} + T_{2L}^2)^{1/2}$, we get

$$dp^2 d\omega^2 = 4M_n q_{1L}(T_{2L}^2 + 2M_n T_{2L})^{1/2}\, dT_{2L} d(\cos\theta_{2L}).$$

If each increment of area $dTd(\cos\theta)$ is now weighted by the appropriate detection efficiency $\eta(T)\,\zeta(\cos\theta)$ for that increment, the effective interval $(\partial p^2 \partial\omega^2)_{jk}$ for data collected in the $\underline{j}$th time bin and the $\underline{k}$th zone is

$$(\partial p^2 \partial \omega^2)_{jk} = 4M_n q_{1L} \int\int (2M_n T_{2L} + T_{2L}^2)^{1/2}\, \eta_j(T_{2L})\, \zeta_k(\cos\theta_{2L}) dT_{2L} d(\cos\theta_{2L}). \qquad \text{(III-4)}$$

The above integrals were all evaluated numerically by using an IBM 7090 computer. The net cross section for each interval $(\partial p^2 \partial \omega^2)_{jk}$ is obtained by combining the data taken with hydrogen target full and delays normal (FN) with the data taken with target full, delays abnormal (FA); target empty, delays normal (EN); target empty, delays abnormal (EA):

$$\frac{\partial^2 \sigma_{jk}}{\partial p^2 \partial \omega^2_{NET}} = \frac{\partial^2 \sigma_{jk}}{\partial p^2 \partial \omega^2_{FN}} - \frac{\partial^2 \sigma_{jk}}{\partial p^2 \partial \omega^2_{EN}} - \frac{\partial^2 \sigma_{jk}}{\partial p^2 \partial \omega^2_{FA}} + \frac{\partial^2 \sigma_{jk}}{\partial p^2 \partial \omega^2_{EA}}. \qquad \text{(III-5)}$$

The statistical errors δ_{jk} on these cross sections are in a similar notation,

$$\delta_{jk} = [(\delta_{jk}^{FN})^2 + (\delta_{jk}^{EN})^2 + (\delta_{jk}^{FA})^2 + (\delta_{jk}^{EA})^2]^{1/2},$$

where δ_{jk}^{FN} is the statistical error on the jkth full-normal cross section, etc. The functions $F_{jk}(p^2, \omega^2)$ to be used in the extrapolation to the pion-pion cross section $\sigma_{\pi\pi}(\omega^2)$ are given by

$$F_{jk}(p^2, \omega^2) = (\overline{p_j^2} + \mu^2)^2 \frac{\partial^2 \sigma_{jk}}{\partial p^2 \partial \omega^2} \left(\frac{M_p}{M_n}\right)^2 \frac{\pi}{f^2} q_{1L}^2 \frac{1}{\left(\overline{\omega_{jk}^2}\right)^{1/2} \left(\overline{\frac{\omega_{jk}^2}{4}} - \mu^2\right)^{1/2}}, \tag{III-6}$$

where the notations $\bar{p}_j$ and $\bar{\omega}_{jk}$ mean that the function has been evaluated at the mean values of p^2 and ω^2 for the jth time bin and the kth θ interval.

C. Corrections to the Data

A number of corrections to the raw data (i.e., those two-pion, one-neutron events that fit the kinematics) were made before the cross sections $d^2\sigma/dp^2 d\omega^2$ and $F(p^2, \omega^2)$ were computed. These corrections were made to take into account the following effects.

1. Pions (from a 2π, 1n final state) that traversed the 6 in. of plastic scintillator in the dish might scatter into adjacent counters or might produce charged particles that scattered into adjacent counters. Our data-processing system would reject such events because there were more than two charged prongs. Thus, the number of events that we measured would be less than the true number.

2. For some 2π, 1n final states of the type we wished to measure, it was kinematically possible for one of the pions to be produced at an angle $\theta < 4^\circ$; such events would go undetected by our counter dish.

3. Final-state neutrons could undergo n-p scattering in the hydrogen target; such neutrons could

(a) come off at an angle $\theta > 60^\circ$ and so avoid detection,

(b) register in the wrong (θ, ϕ) interval so that kinematics would not be satisfied,

(c) register in the wrong time bin so that if kinematics were satisfied, the distribution of events in p^2 and ω^2 would be incorrectly augmented.

To account for pion rescattering in the dish, a Monte Carlo calculation was done to obtain the probability that a pion traversing a counter in a given θ ring in the dish would produce a count in an adjacent counter. Since plastic scintillator is 98% CH, measured[17] pion-carbon and pion-proton cross sections were used to determine the history of the pion going through the plastic. Seven probabilities $P(\theta_j)$ were generated, one for each θ ring in the dish. The probability for a pion to rescatter in one of the counters in the array extending from 60° to 147° was assumed to be zero because of the small thickness of plastic in these counters. Thus, one could define a set $P(\theta_j) = 0$, $j = 8, 11$. Then each event with a $2\pi^-$ signature that satisfied kinematics was counted not as one event but as $1/[1-P(\theta_{\pi 1})][1-P(\theta_{\pi 2})]$ events, where $\theta_{\pi 1}$ and $\theta_{\pi 2}$ are the θ rings in which the pions landed.

The correction for neutron rescattering in the hydrogen target was also done by a Monte Carlo method[18] with the use of known n-p total cross sections and angular distributions.[19] This calculation determined what percentage of "good fit" events with a given time bin and neutron angle $\tau_i\theta_j$ would, if scattered into a $\tau_r\theta_s$, still satisfy kinematics, and how many would get scattered out of the dish. The result was a set of 49 numbers a_{ij} such that if N_{ij} were the observed number of events in time bin i and θ ring j, then $(N_{ij})_{TRUE} = (N_{ij})_{OBS} \times a_{ij}$. In order to correct the measured cross sections for those events that went undetected owing to effect No. 2, the "good fit" events were binned into five equal intervals of ω^2 between the kinematically allowed limits (see Fig. 3). For each of these intervals, the search values of the variables of an event were used to obtain $\cos\theta^*_{13}$ and $\cos\theta^*_{14}$, that is, the cosine of the angle between the incident pion and one of the final-state pions as measured in the barycentric frame of the two final-state pions. This barycentric system has total invariant energy ω. Calling P_1 and P_3 the four-momenta of the incident pion and one of the final-state pions, respectively, we form the invariant scalar product

$$P_1 \cdot P_3 = \omega_{1L}\omega_{3L} + q_{1L}q_{3L}\cos\theta_{13L} = \omega_{1B}\omega_{3B} + \pi_{1B}q_{3B}\cos\theta^*_{13B},$$

where the subscripts L and B refer to laboratory and barsy systems, respectively, and where

$$\cos\theta^*_{13B} = \frac{\cos\theta_{13L} q_{1L} q_{3L} + \omega_{3L}\omega_{1L} - \omega_{3B}\omega_{1B}}{q_{1B}\, q_{3B}}, \quad \omega_{3B} = \omega/2,$$

and

$$\omega_{1B} = [\omega^2 + \mu^2 + (M_p/M_n)p^2 - (M_p - M_n)^2]/2\omega.$$

Angular distributons $N(\cos\theta^*)$ were determined for each of the ω^2 intervals. These distributions were used as weighting factors to generate the laboratory coordinates of 2π, 1n events, starting with a fixed p^2 and ω^2, and varying $\cos\theta^*$ between +1 and -1. For each of the 49 pairs (p_j^2, ω_{jk}^2) the fraction of events for which $\theta_{lab}^{pion} < 4^o$ was determined. The cross sections were then corrected accordingly.

D. Results

The corrected cross sections obtained for the reaction $\pi^+ + p \rightarrow \pi^+ + \pi^+ + n$ at incident pion momenta of 1.25 and 1.75 BeV/c are given in Tables VI and VII. The entries in the tables are the cross sections $F_{ij}(p^2, \omega^2)$ (in millibarns) for each of the momentum transfers p^2 and π-π barycentric energies ω^2. Each row is at a fixed p_j^2, as indicated. The errors shown are the rms statistical errors. In order to find $\sigma_{\pi\pi}(\omega^2)$ by the extrapolation method, the $F_{ij}(p^2, \omega^2)$ at fixed p^2 were fitted to polynomials in ω^2 by using a least-squares fitting procedure. The values of $F(p^2, \omega^2)$ used in the extrapolation [i.e., the curves $F(p^2, \omega^2)$ vs p^2 holding ω^2 fixed] were taken from the best-fit polynomials. Plots of $F(p^2, \omega^2)$ vs p^2 are given in Figs. 11 and 12. According to the single-pion-exchange model, the value of $\sigma_{\pi\pi}(\omega_k^2)$ is given by $\sigma_{\pi\pi}(\omega_k^2) = -F(p^2, \omega^2)$ at $p^2 = -\mu^2$.

To find the distribution of events as a function of ω^2 only, we have integrated the $\partial^2\sigma/\partial p^2 \partial \omega^2$ over p^2. In Fig. 13 we show a plot of

$$d\sigma/d\omega^2 = \int \frac{\partial^2\sigma}{\partial p^2 \partial \omega^2}\, dp^2 . \qquad \text{(III-7)}$$

Table VI. Values of the cross sections $F(p^2, \omega^2)$(in mb) used in determining $\sigma_{\pi\pi}$ by the extrapolation method. The incident pion momentum is 1.25 BeV/c. Each entry gives ω^2/μ^2, $F(p^2, \omega^2)$ and δF_{rms}.

Time bin	θ Zone						
	1	2	3	4	5	6	7
1	29.190	28.010	26.060	23.390	20.040	16.090	11.600
	22.741	76.925	82.882	56.479	39.388	49.666	27.878
	18.197	8.197	7.902	6.559	6.151	6.964	8.179
2	26.010	25.020	23.400	21.170	18.390	15.100	11.360
	84.686	11.339	94.624	63.641	42.734	54.926	34.375
	28.438	12.063	9.272	8.167	7.448	7.828	9.412
3	23.810	22.940	21.520	19.560	17.100	14.210	10.920
	59.696	71.267	68.842	32.064	47.029	24.225	9.651
	30.095	12.179	9.980	8.272	6.833	7.293	8.774
4	21.870	21.100	19.830	18.090	15.910	13.340	10.420
	20.188	38.810	48.042	37.847	36.222	18.731	9.720
	40.406	17.768	13.599	10.020	8.266	10.131	11.045
5	19.700	19.030	17.920	16.410	14.520	12.280	9.740
	25.673	39.386	49.325	20.772	23.371	13.031	40.875
	35.808	15.075	11.198	10.579	8.463	9.329	8.960
6	17.690	17.110	16.150	14.840	13.190	11.240	9.035
	34.019	36.584	20.060	34.770	19.938	2.905	2.272
	42.693	15.602	12.345	9.425	7.812	9.504	9.706
7	15.610	15.110	14.290	13.160	11.750	10.090	8.195
	32.486	4.300	10.940	6.240	14.336	12.466	0.908
	23.526	15.429	12.608	10.570	8.593	11.636	11.467

Table VII. Values of the cross sections $F(p^2, \omega^2)$ in mb used in determining $\sigma_{\pi\pi}$ by the extrapolation method. The incident pion momentum is 1.75 BeV/c. Each entry gives ω^2/μ^2, $F(p^2/\mu^2, \omega^2/\mu^2)$ and δF_{rms}.

Time bin	θ Zone 1	2	3	4	5	6	7
1	42.560	40.910	38.180	34.440	29.750	24.210	17.930
	58.055	52.354	57.192	41.296	34.197	18.534	62.698
	12.583	7.113	6.022	5.428	5.286	5.576	6.935
2	37.480	36.100	33.830	30.710	26.810	22.200	16.970
	57.123	72.041	51.111	44.632	40.410	45.719	32.078
	17.222	9.483	8.639	6.577	5.816	5.628	7.012
3	34.090	32.880	30.880	28.130	24.700	20.640	16.040
	24.178	51.596	54.773	29.570	31.057	14.927	19.641
	18.908	10.461	9.125	7.645	5.278	6.384	6.935
4	31.130	30.050	28.280	25.840	22.790	19.190	15.100
	56.967	53.664	36.420	43.069	29.756	15.150	34.837
	24.434	12.699	11.261	8.401	7.212	7.643	8.780
5	27.870	26.930	25.390	23.270	20.620	17.490	13.930
	15.707	9.021	23.232	21.989	33.459	16.526	10.293
	22.074	12.628	10.921	8.740	6.378	6.943	7.494
6	24.890	24.080	22.740	20.900	18.590	15.870	12.780
	2.676	33.350	10.928	6.571	32.478	14.363	4.552
	27.913	11.253	9.126	9.498	6.340	7.599	9.339
7	21.850	21.150	20.000	18.420	16.450	14.110	11.470
	21.187	17.018	18.585	4.516	14.972	11.346	11.764
	29.099	12.655	11.141	8.631	7.065	8.078	7.678

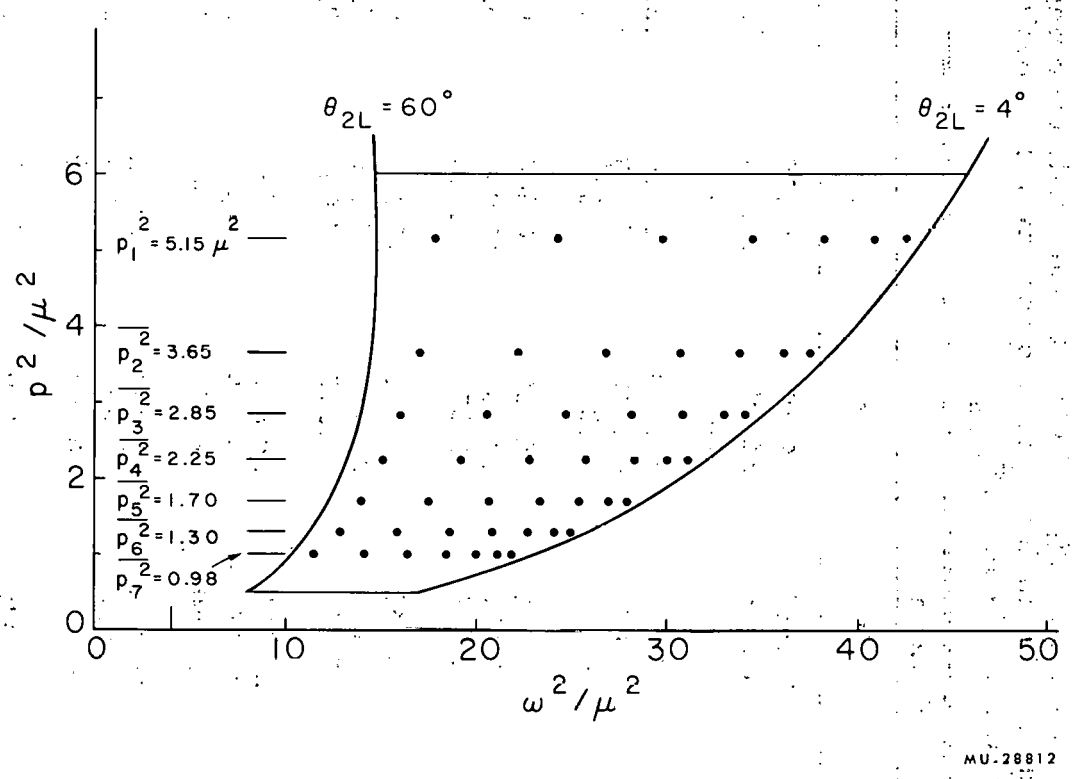

Fig. 11. Plot of (ω^2, p^2) region showing mean values $(\omega^2/\mu^2, p^2/\mu^2)$ at which $\partial^2\sigma/(\partial p^2/\mu^2\ \partial\omega^2/\mu^2)$ were evaluated.

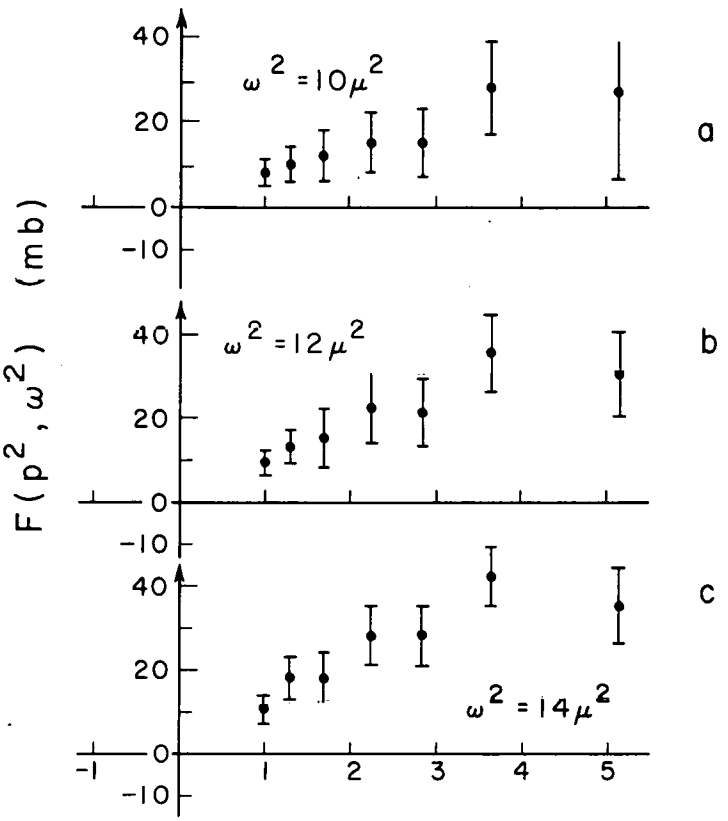

MU-28813

Fig. 12a, b, c. Extrapolation plots of $F(p^2, \omega^2)$, where $\sigma_{\pi\pi}(\omega^2) = - F(p^2, \omega^2)$ at $p^2/\mu^2 = -1$.
The data shown are for incident-pion momentum of 1.25 BeV/c.

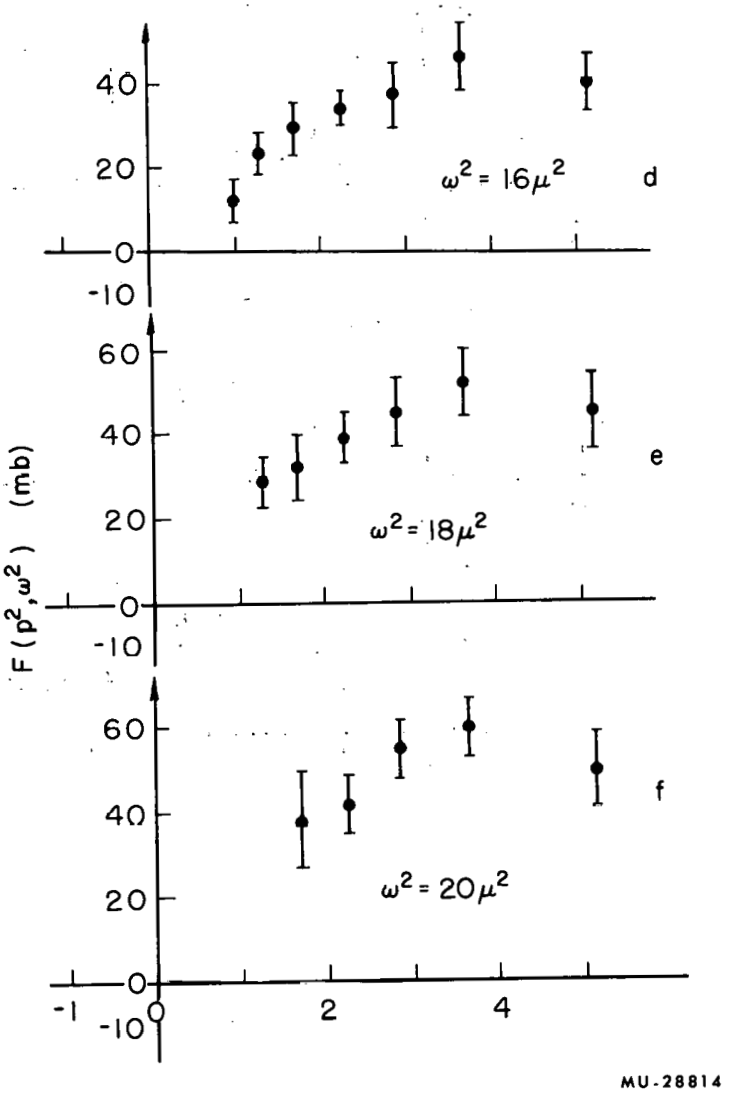

Fig. 12d,e,f. Extrapolation plots of $F(p^2,\omega^2)$, where $\sigma_{\pi\pi}(\omega^2) = -F(p^2,\omega^2)$ at $p^2/\mu^2 = -1$.
The data shown are for incident-pion momentum of 1.25 BeV/c.

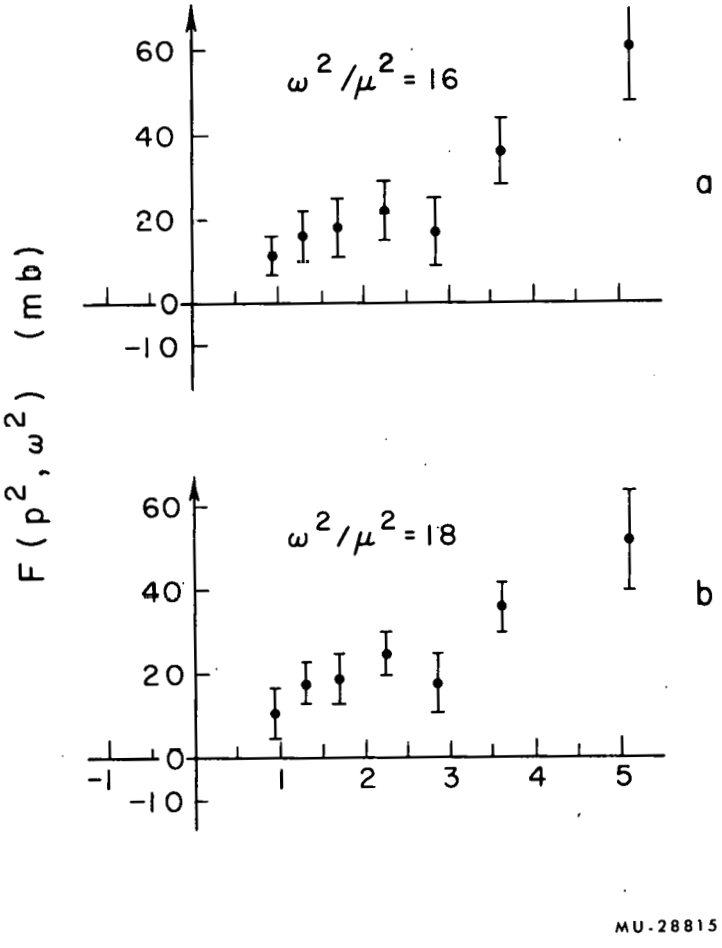

Fig. 13a, b. Extrapolation plots of the function $F(p^2, \omega^2)$. The incident pion momentum is 1.75 BeV/c; $\sigma_{\pi\pi}(\omega^2) = -F(p^2, \omega^2)$ at $p^2/\mu^2 = -1$.

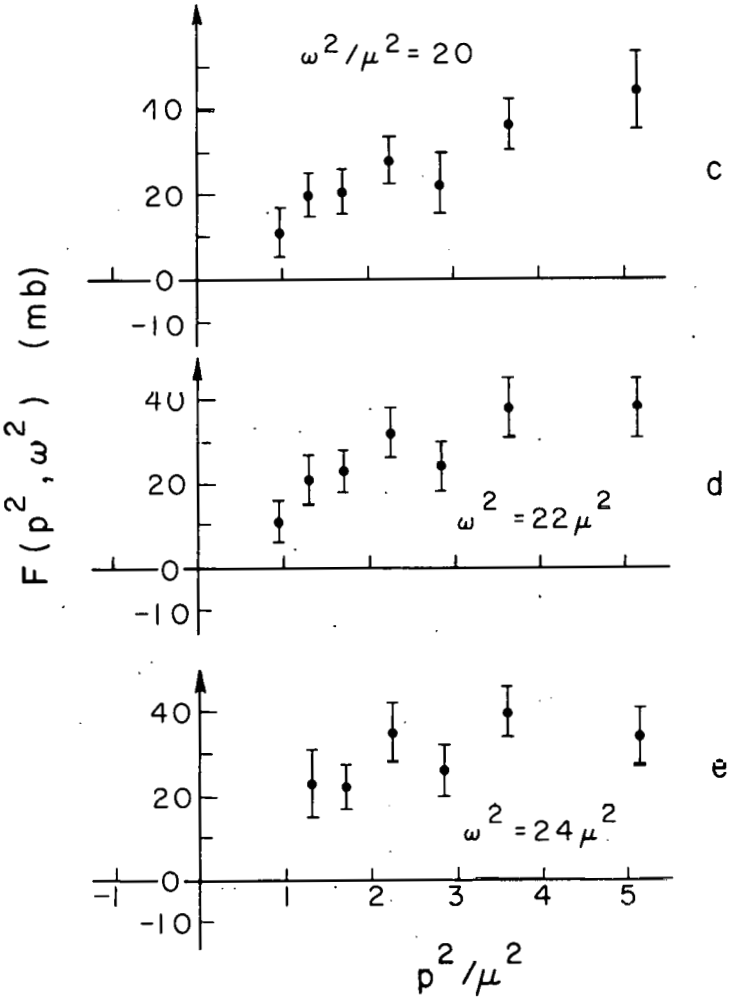

Fig. 13c,d,e. Extrapolation plots of the function $F(p^2, \omega^2)$. The incident pion momentum is 1.75 BeV/c; $\sigma_{\pi\pi}(\omega^2) = -F(p^2, \omega^2)$ at $p^2/\mu^2 = -1$.

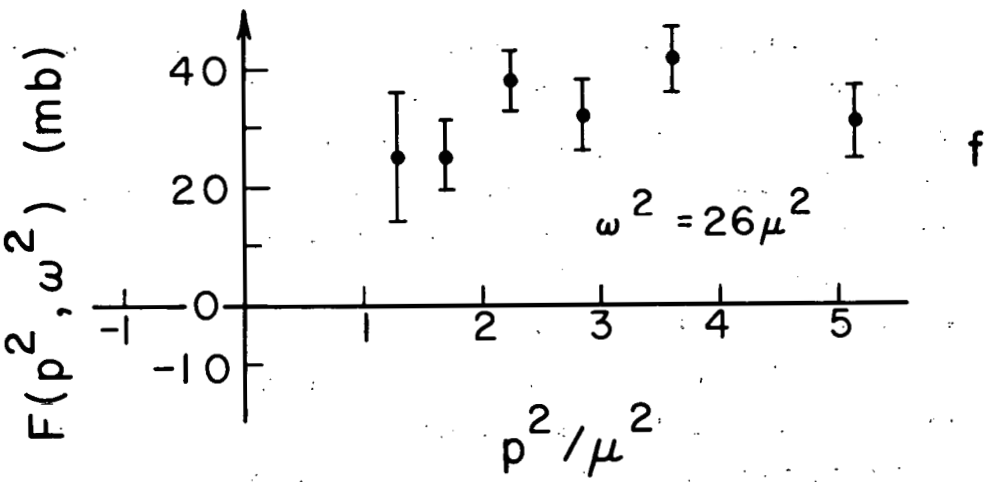

MU-28817

Fig. 13f. Extrapolation plots of the function $F(p^2, \omega^2)$. The incident pion momentum is 1.75 BeV/c; $\sigma_{\pi\pi}(\omega^2) = -F(p^2, \omega^2)$ at $p^2/\mu^2 = -1$.

If the scattering amplitude for single-pion production were really dominated by the contribution from the pole at $p^2 = -\mu^2$, then the limit relation

$$\lim_{p^2 \to -\mu^2} \frac{\partial^2 v}{\partial p^2 \partial \omega^2} \to \frac{f^2}{2\pi} \frac{p^2/\mu^2}{(p^2+\mu^2)^2} \frac{\omega(\frac{1}{4}\omega^2 - \mu^2)^{1/2}}{q_{1L}^2} \sigma_{\pi^+\pi^+} \qquad \text{(III-8)}$$

could perhaps be replaced by an equation valid over a range of $p^2 > 0$, i.e., a range of p^2 that is physically observable. One would expect, for example, that for this range of p^2 the extrapolation plots would be linear and would pass through the origin $F(p^2, \omega^2) = 0$ at $p^2 = 0$. If this were the case, the $\sigma_{\pi\pi}(\omega)$ for several values of ω could be obtained from this equation by integration over p^2 within suitable limits. For each value of $\omega_{\pi\pi}$ for which the integration is done, the minimum value of p^2 is determined by the kinematics. The maximum value is the cutoff value discussed in the introduction.

In Fig. 14 we show the results of such an integration. We wish to point out here that the inclusion of the results of this calculation is done, in a certain sense, for completeness. It will be shown in the following sections that the data we have taken are not consistent with the hypothesis that the single-pion-exchange pole gives rise to the dominant contribution to the scattering in single-pion production. In order to investigate interference with, or departure from, one-pion exchange in the reaction $\pi^+ + p \to \pi^+ + \pi^+ + n$, the data were analyzed in two ways.

The first way was to calculate for each event the invariant barycentric-energy squared, $\omega_{\pi n}^2$, of the neutron with each of the final-state pions. There were two values of $\omega_{\pi n}^2$ associated with an event because the final-state pions are indistinguishable; thus

$$\omega_{\pi_3 n}^2 = (\omega_{\pi_3} + \omega_n)^2 - (\vec{q}_{\pi_3} + \vec{p}_n)^2 \qquad \text{(III-9)}$$

$$= (\omega_{\pi_3} + \omega_n)^2 - (q_{1L}^2 + q_{\pi_4}^2 - 2 q_{1L} q_{\pi_4} \cos\theta_{14L}),$$

where all quantities are in the laboratory frame. Subscripts 3 and 4 denote final-state pions; 1L denotes incident pion.

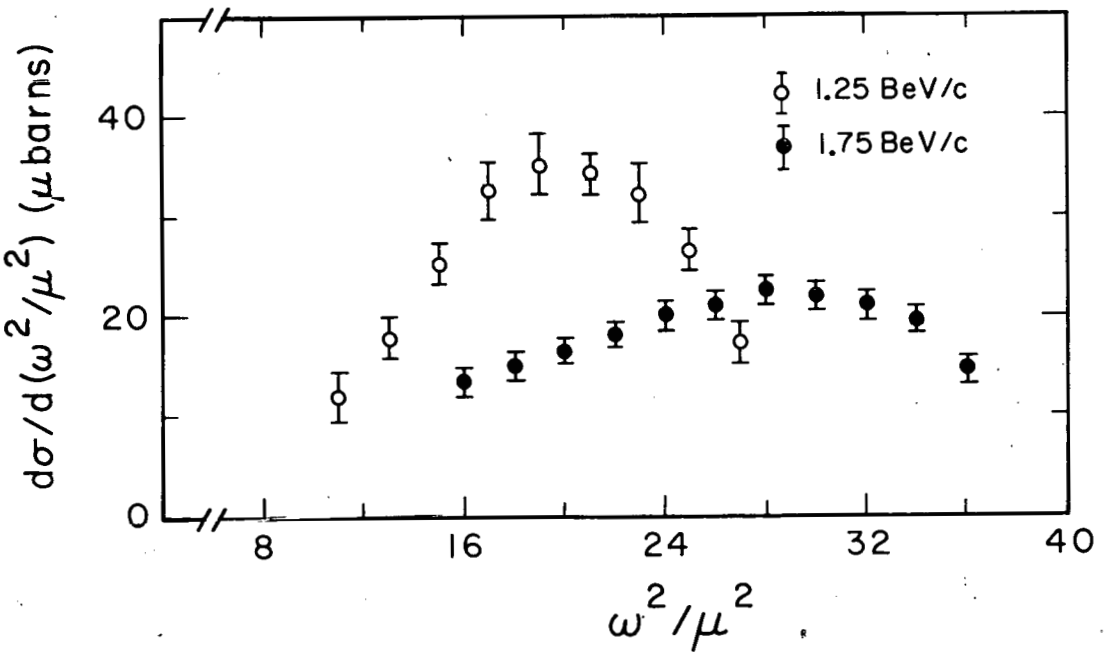

Fig. 14. Differential cross section $d\sigma/d(\omega^2/\mu^2)$ for incident-pion momenta of 1.25 and 1.75 BeV/c.

The distribution of events as a function of $\omega^2_{\pi n}$ is shown in Fig. 15. The positions, isotopic spin, and angular momentum of the known pion-nucleon resonances are also shown. In order to investigate in some detail the possible effect on our data of pion-nucleon interactions, we have made the distributions $N(\omega^2_{\pi n})$ for events in each of the seven momentum-transfer intervals. The results are shown in Figs. 16 and 17.

The second type of analysis was done on the basis of a suggestion by Yang and Treiman.[20] If the reaction $\pi^+ + p \rightarrow \pi^+ + \pi^+ + n$ takes place through single-pion exchange i.e., the exchange of a particle with spin = 0, then all orientations of the plane of the two final-state pions about the 3 momentum $\vec{p}$ of the virtual particle should occur with equal probability.

Transforming to the rest frame of the incident pion, let $\hat{q}_{\pi 3}$ and $\hat{q}_{\pi 4}$ be unit vectors in the directions of the three-momenta of the final-state pions and let $\hat{p}_p$ and $\hat{p}_n$ be unit vectors along the proton and neutron three-momenta.

Then $\hat{k}_{pn} = \hat{p}_p \times \hat{p}_n$ and $\hat{k}_{\pi\pi} = \hat{q}_{\pi 3} \times \hat{q}_{\pi 4}$ are unit normals to the p-n and π-π planes, and one determines the distribution in separation angle $\phi = \cos^{-1}(\hat{k}_{pn} \cdot \hat{k}_{\pi\pi})$. Distributions are shown for events in each of the time bins (momentum-transfer intervals) 1 through 7 in Figs. 18 and 20.

E. Errors

The errors that have been presented in the tables and figures have been statistical (rms) errors on the number of events compounded from the data taken at conditions target full, delays normal; target empty, delays normal, etc.

Of the other possible sources of error, one was the muon contamination of the incident beam. This was probably of the order of 3%,[7] and would tend to raise all cross sections by the same amount, leaving the shapes of all distributions unchanged. Another possible source of error may have been the assumption that the time-bin efficiency curves were the same for all θ zones. The neutron-counting efficiency was measured for a large number of neutron energies only for θ zone No. 5.

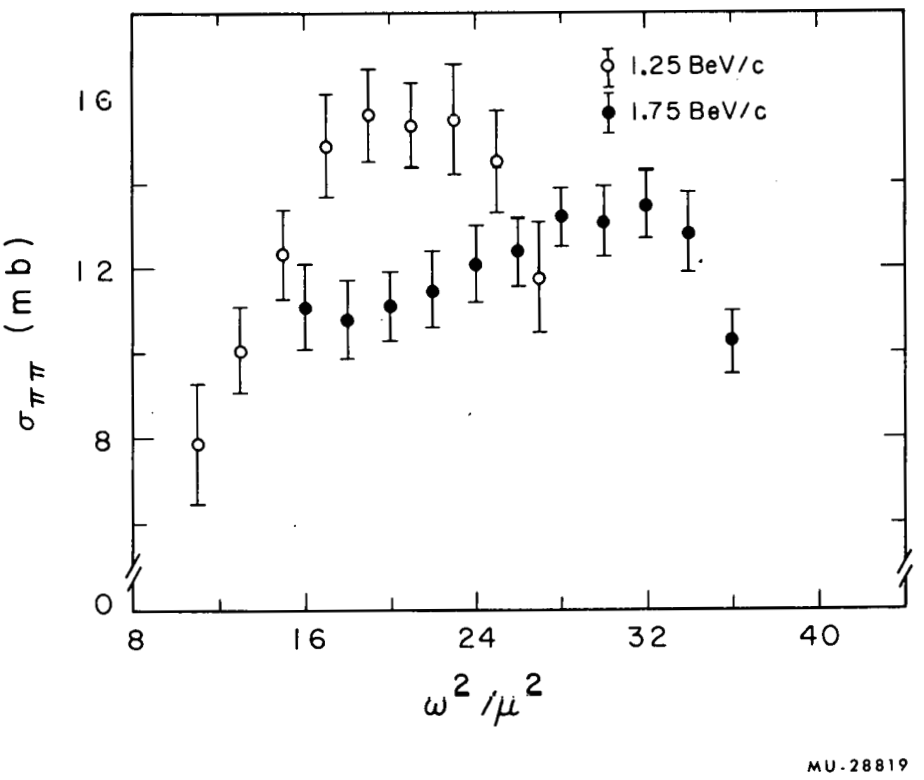

Fig. 15. $\sigma_{\pi\pi}$ obtained by integration of Eq. (III-8) over p^2 in the physical region. The data shown are for incident pion momenta of 1.25 and 1.75 BeV/c.

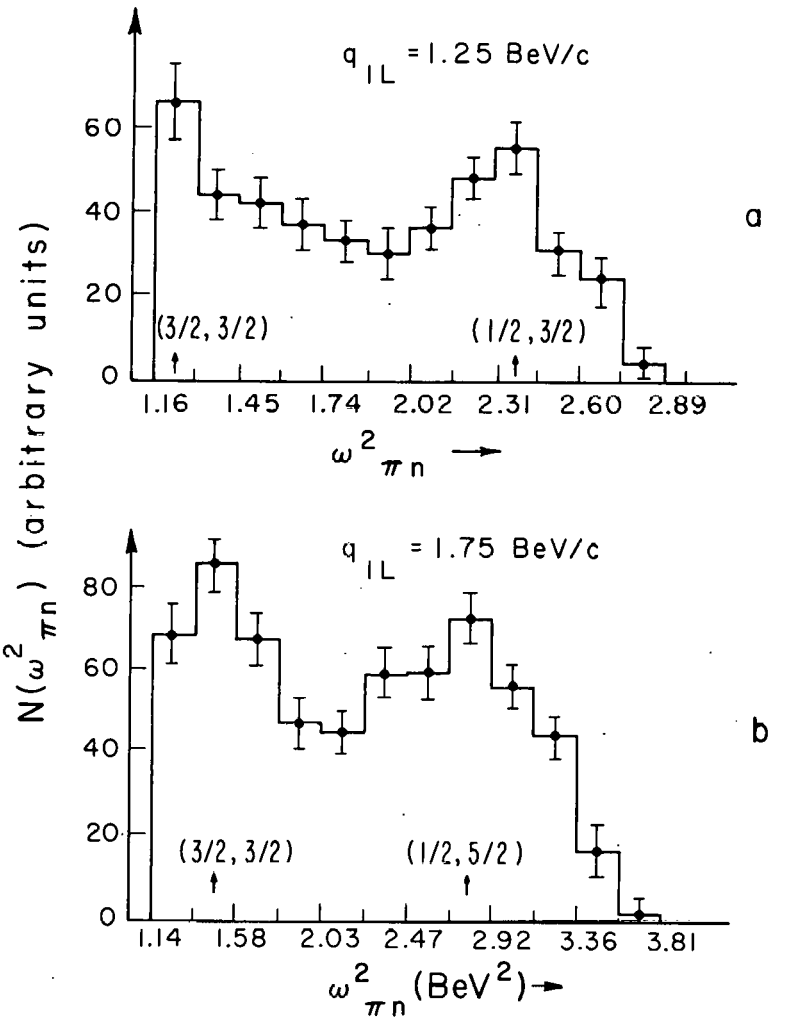

Fig. 16a,b. Distribution of events as a function of the square of the barycentric energy $\omega^2_{\pi n}$ of the pion and nucleon in the final state. The momentum of the incident pion is denoted by q_{1L}. Events were sorted into 12 equal intervals $\Delta\omega^2_{\pi n}$ = 0.222 BeV^2. The arrows show the positions of the (3/2, 3/2), (1/2, 3/2) and (1/2, 5/2) pion-nucleon resonances.

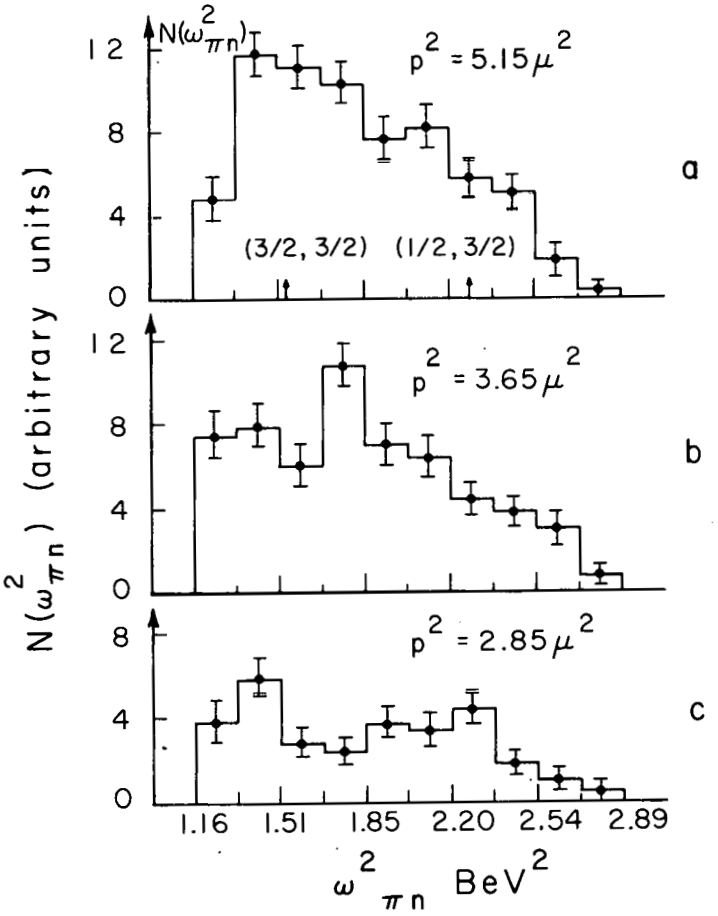

Fig. 17a,b,c. The distribution $N(\omega^2_{\pi n})$ for events in each of the seven momentum-transfer intervals into which the data was binned. The mean values of p^2 are shown in the graphs. The incident-pion momentum was 1.25 BeV/c. Events were sorted into ten equal intervals $\Delta\omega^2_{\pi n} = 0.173$ BeV^2. Arrows give the position of the (3/2, 3/2) and (1/2, 3/2) pion-nucleon resonances.

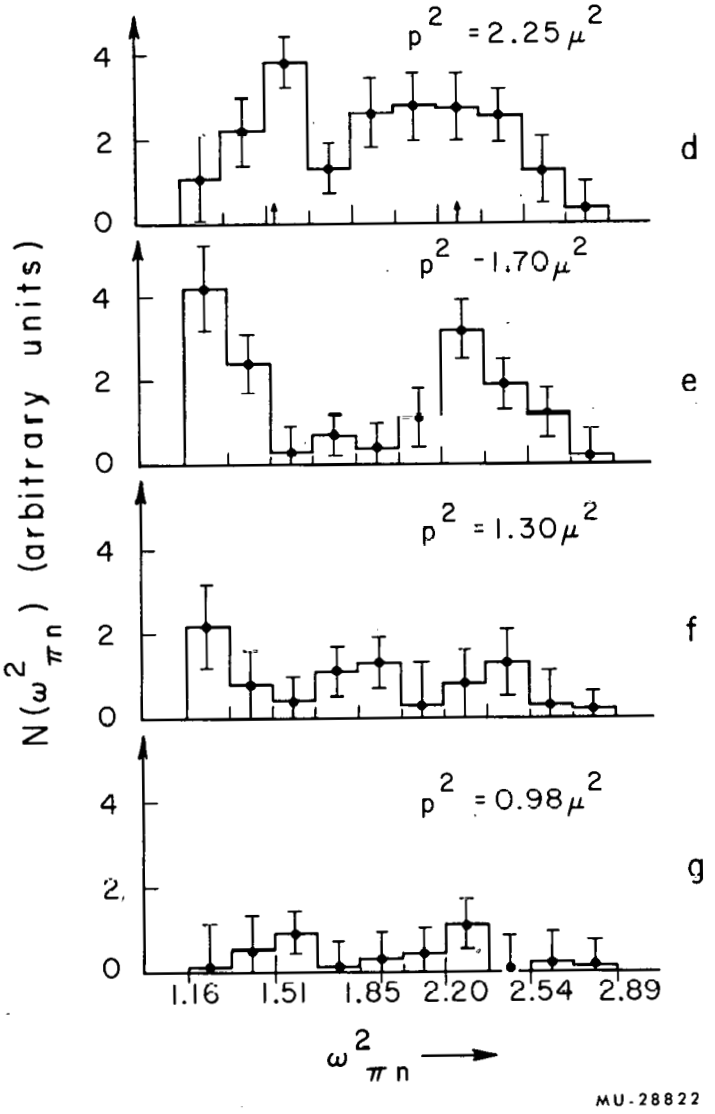

Fig. 17d,e,f,g. The distribution $N(\omega^2_{\pi n})$ for events in each of the seven momentum-transfer intervals into which the data was binned. The mean values of p^2 are shown in the graphs. The incident-pion momentum was 1.25 BeV/c. Events were sorted into ten equal intervals $\Delta\omega^2_{\pi n} = 0.173$ BeV^2. Arrows give the position of the (3/2, 3/2) and (1/2, 3/2) pion-nucleon resonances.

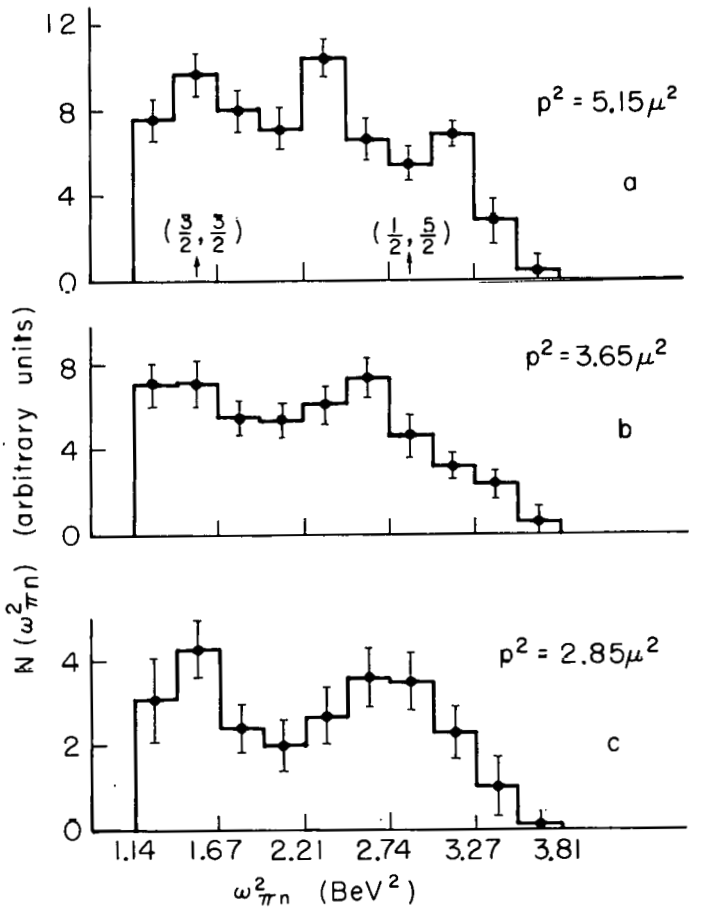

MU-28823

Fig. 18a,b,c. The distribution $N(\omega^2_{\pi n})$ for events in each of the time bins. The incident-pion momentum is 1.75 BeV/c. Arrows show the positions of the (3/2, 3/2) and (1/2, 5/2) pion-nucleon resonances. Events were sorted into 10 equal intervals $\Delta\omega^2_{\pi n} = 0.267$ BeV^2.

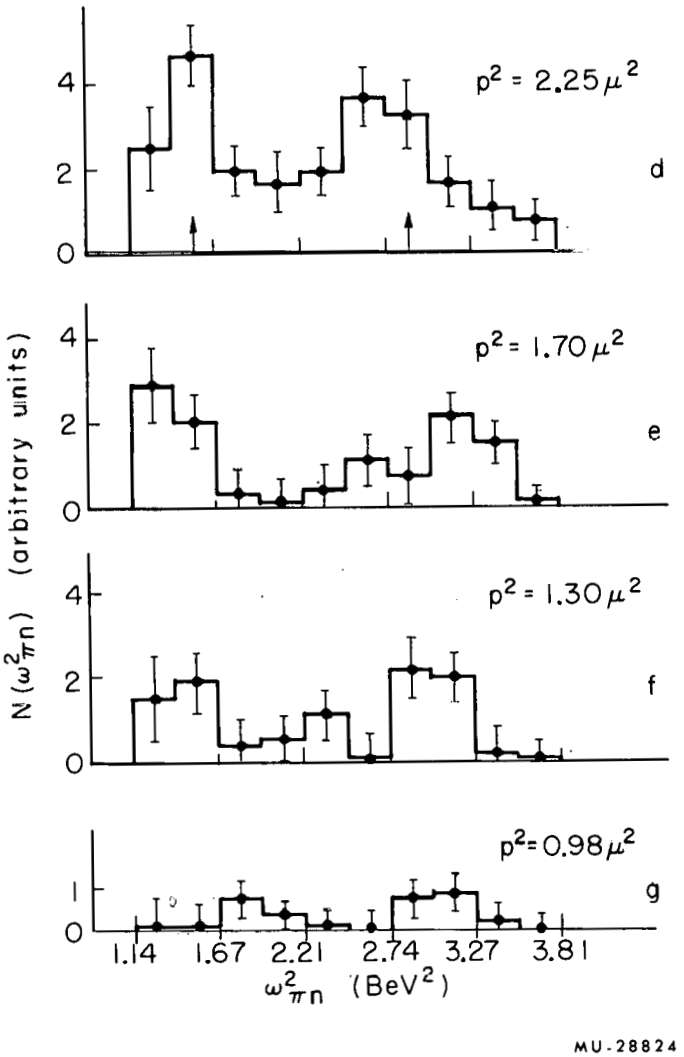

Fig. 18d,e,f,g. The distribution $N(\omega^2_{\pi n})$ for events in each of the time bins. The incident-pion momentum is 1.75 BeV/c. Arrows show the positions of the (3/2, 3/2) and (1/2, 5/2) pion-nucleon resonances. Events were sorted into 10 equal intervals $\Delta\omega^2_{\pi n} = 0.267$ BeV^2.

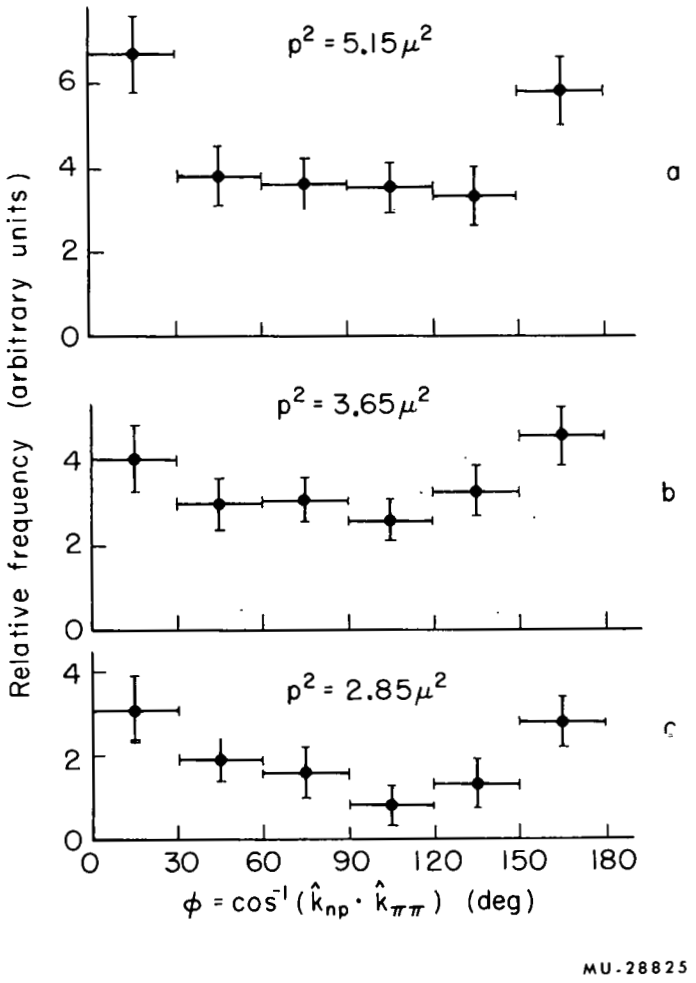

Fig. 19a,b,c. The Yang-Treiman Test. Relative frequency of occurrence of the separation angle ϕ between the normals $\hat{k}_{pn}$ and $\hat{k}_{\pi\pi}$, where $\hat{k}_{pn}$ is the unit normal to the proton-neutron scattering plane and $\hat{k}_{\pi\pi}$ is the unit normal to the plane of the two final-state pions. All quantities are defined in the rest frame of the incident pion. The incident pion momentum (lab frame) is 1.25 BeV/c.

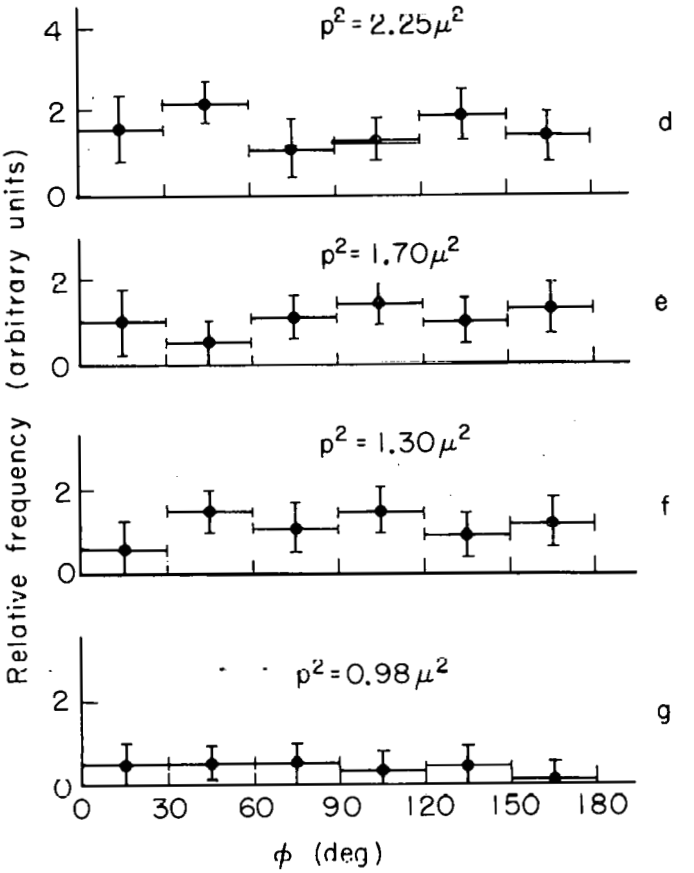

Fig. 19d,e,f,g. The Yang-Treiman Test. Relative frequency of occurrence of the separation angle ϕ between the normals $\hat{k}_{pn}$ and $\hat{k}_{\pi\pi}$, where $\hat{k}_{pn}$ is the unit normal to the proton-neutron scattering plane and $\hat{k}_{\pi\pi}$ is the unit normal to the plane of the two final-state pions. All quantities are defined in the rest frame of the incident pion. The incident pion momentum (lab frame) is 1.25 BeV/c.

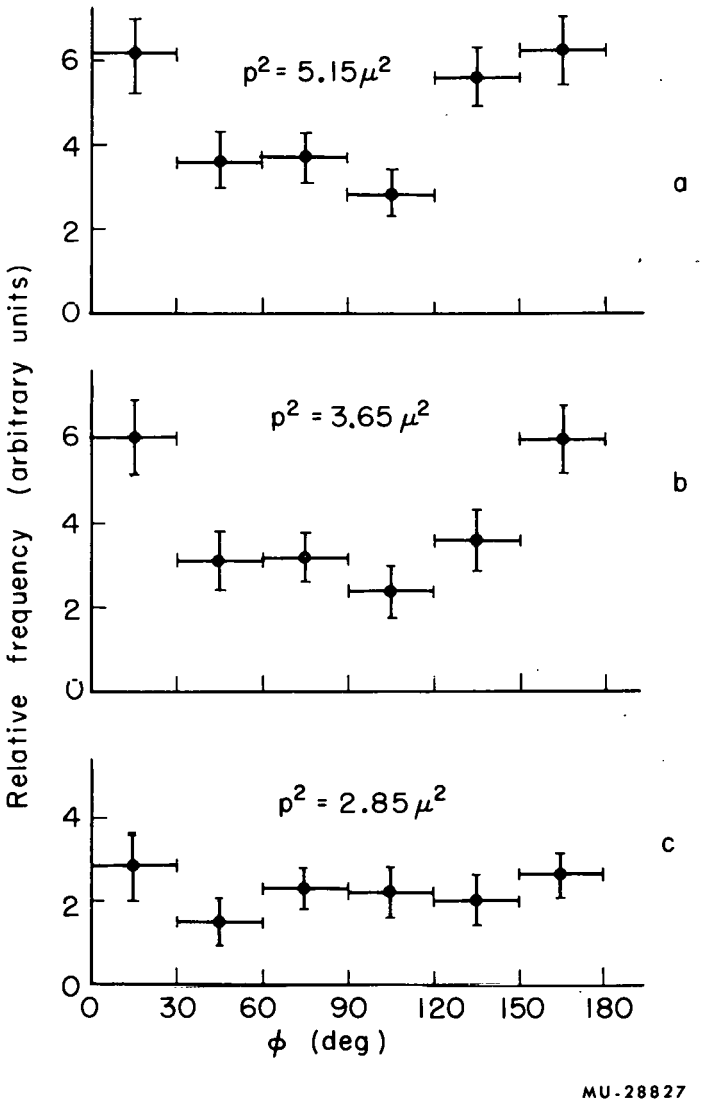

Fig. 20a,b,c. The Yang-Treiman test for data taken with an incident pion momentum of 1.75 BeV/c.

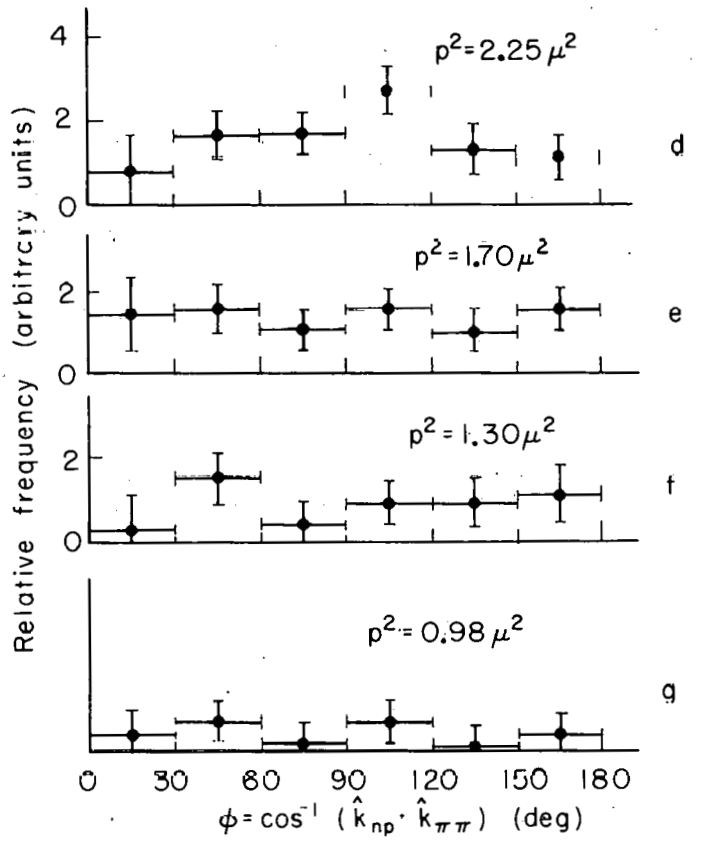

Fig. 20d,e,f,g. The Yang-Treiman test for data taken with an incident pion momentum of 1.75 BeV/c.

Measurements at only a few neutron energies were taken with a zone No. 2 counter, and the overall efficiency for this counter ($\eta = \eta_{\tau_0} + \eta_{\tau_1} + \eta_{\tau_7} + \eta_{\tau_{00}}$) was, within statistics, equal to that for the zone No. 5 counter. However, because the time available for making the measurements was limited, it was not possible to accumulate sufficient data to allow a comparison of the efficiencies η_{τ_j} (zone No. 2) with η_{τ_j} (zone No. 5) for each of the incident neutron energies used in the neutron-efficiency calibration. The efficiency for θ zones 1, 3, and 6 was not measured at all. The neutron-counting efficiency of a θ zone No. 7 counter was measured for only three values of incident neutron energy. The efficiencies obtained were in fair agreement with those obtained for θ zones No. 2 and No. 5. If the efficiencies $\eta_j(T_{2L})$ for a given time bin were not the same for all θ zones, this would alter both the magnitude and the shape of the distributions $\partial^2\sigma/\partial p^2 \partial\omega^2$ vs ω^2, since (a) the values $(\partial p^2 \partial \omega^2)_{jk}$ would be changed (see Eq. III-4), and (b) the values $\overline{\omega^2}_{jk}$ and $\overline{p^2}_j$ would be changed (Eqs. III-2 and III-1). It is extremely difficult to estimate the magnitude of such a possible error, since one would have to assume values of $\eta_j(T_{2L})$ for the unmeasured θ zones for all time bins $j = 1, 7$ and perform a great many integrations to determine the change in $(\partial p^2 \partial \omega^2)_{jk}$ as a function of the η_j. The agreement we obtained for a few energies between θ zones No. 2, No. 5, and No. 7 leads us to believe that the differences in efficiency, if present, were small.

Another source of error was connected with the search program. It (the program) did not make a search when, for a 2π, ln event, the neutron and pion landed in the same counter. The number of good events lost this way amounted to a 3% decrease in total cross section.[7]

Also, when the fitting program was tested with 600 events generated from kinematics programs, it failed to find kinematic fits for approx 1% of them, so that the error from this source was quite small.

The loss of events (undetected events) due to pions coming off in the polar angular interval $147^\circ \leq \theta \leq 180^\circ$ has been accounted for by including them in the calculations for loss of events for pions in the interval $0^\circ \leq \theta \leq 4^\circ$.

F. Discussion of Results

We wish to recall at this point that the Yang-Treiman analysis allows only one inference to be made, i.e., that a deviation from isotropy implies a process other than or in addition to the exchange of a virtual spinless particle (a pion in our case) between the incident particle and the target system. In the reaction $\pi + p \rightarrow \pi + \pi + n$, there could be processes other than single-pion exchange, such as isobar formation or three-pion exchange. Even in one-pion exchange, it is possible to have final-state pion-nucleon interactions take place (see Fig. 1). Isotropy, on the other hand, does not imply single-pion exchange; it is simply consistent with it.

Our data (Figs. 18, 19) indicate that for incident pion momentum $q_{1L} = 1.25$ BeV/c the distributions for $p^2 = 2.85\mu^2$, $3.65\ \mu^2$, and $5.15\ \mu^2$ are anisotropic. At $q_{1L} = 1.75$ BeV/c, the distributions for $p^2 = 3.65\ \mu^2$ and $5.15\ \mu^2$ are anisotropic. The curves at the other values of p^2 seem, within statistics, to be isotropic. Thus, if we were to try to obtain pion-pion cross sections from our data by the extrapolation method, we would have to restrict ourselves to using points at $p^2 = 0.98$, 1.30, 1.70, and $2.25\mu^2$ for $q_{1L} = 1.25$ BeV/c and $p^2 = 0.98$, 1.30, 1.70, 2.25, and $2.85\ \mu^2$ for $q_{1L} = 1.75$ BeV/c. The points at these values of p^2 would at least be consistent with single-pion exchange on the basis of the Yang-Treiman analysis. However, if we look at the curves of $N(\omega^2_{\pi n})$ vs $\omega^2_{\pi n}$ for each of the time bins (Figs. 16 and 17) (momentum transfer intervals), there is some indication (even with the poor statistics) of peaking of the distributions at the positions of the pion-nucleon resonances. In particular, at $q_{1L} = 1.25$ BeV/c there is enhancement at the (1/2, 3/2-) resonance ($\omega^2_{\pi n} = 2.28$ BeV/c) for $p^2 = 1.70$ and $2.25\mu^2$. At $q_{1L} = 1.75$ BeV/c, there is enhancement at the (3/2, 3/2+) and (1/2, 5/2+) resonances ($\omega^2_{\pi n} = 1.53$ and 2.82 BeV^2, respectively) for $p^2 = 2.25$ and $2.85\ \mu^2$.

Thus, even at those momentum transfers to the nucleon for which the Yang-Treiman curves seem isotropic, there may be interference between the pion-pion interaction and a final-state pion-nucleon interaction. Since the extrapolation method does not take such

interferences into account, we have not presented values of $\sigma_{\pi\pi}$ based on our extrapolation plots. If one attempts the extrapolations using only data τ_3 through τ_7 at 1.75 BeV/c and τ_4 through τ_7 at 1.25 BeV/c (i.e., consistent with single-pion exchange), the $\sigma_{\pi\pi}$ so obtained either are negative (i.e., the extrapolation fails completely), or are consistent with zero.

At both 1.25 and 1.75 BeV/c incident momenta, the curves are generally nonlinear, and the trend is for the $\sigma_{\pi\pi}$ to be small or zero for the lowest values of ω^2 and to become negative as ω^2 increases. It should be clear that for the range of p^2 investigated in this paper, the exclusion of two or three data points from an extrapolation curve makes the $\sigma_{\pi\pi}$ determination subject to large errors because of the statistics on the data points.

There is no indication from the $d\sigma/d\omega^2_{\pi^+\pi^+}$ curves that resonances exist in the I = 2 dipion system within the energy interval investigated $10\,\mu^2 \leq \omega^2_{\pi\pi} \leq 40\,\mu^2$. We mention this because the same apparatus used in this experiment has been used to investigate the reaction $\pi^- + p \rightarrow \pi^+ + \pi^- + n$ at 1.25 and 1.75 BeV/c, and the $d\sigma/d\omega^2$ for the $(\pi^+\pi^-)$ final state does show the ρ meson even though plots of $N(\omega^2_{\pi^+\pi^-})$ show peaking at the (3/2, 3/2) and (1/2, 5/2) resonances. The point here is that the interference of pion-nucleon with pion-pion interactions did not mask the presence of the ρ meson. The same behavior [i.e., ρ-meson peak in the $N(\omega^2_{\pi^+\pi^0})$ plot and (3/2, 3/2) and (1/2, 5/2) peaks in the $N(\omega^2_{\pi p})$ plots] has been seen in the reaction $\pi^+ + p \rightarrow \pi^+ + \pi^0 + p$.[21]

Kirz et al.[22] have tried to get $\sigma_{\pi^+\pi^+}$ for $4\,\mu^2 \leq \omega^2_{\pi\pi} \leq 6\,\mu^2$ and $6\,\mu^2 \leq \omega^2_{\pi\pi} \leq 8.5\,\mu^2$ by using the extrapolation method on data from the reaction $\pi^+ + p \rightarrow \pi^+ + \pi^+ + n$ with an incident-pion kinetic energy of 357 MeV. They looked at events in the same p^2 range as we used, and the extrapolation method failed in their case even though at their incident-pion energy, the maximum $\omega^2_{\pi^+ n}$ in the final state is below the (3/2,3/2) resonance. It may be, then, that the influence of pion-nucleon resonance interactions is responsible only in part for the failure of the extrapolation method as applied in our work. It is possible, for example, that the extrapolation method would work for smaller momentum transfers than have been used here.

ACKNOWLEDGMENTS

I wish to thank my co-workers Dr. Thomas Ypsilantis, Dr. Clyde Wiegand, Dr. William B. Johnson, Dr. Joseph Lach, and Dr. Tom Eliof. Working with them has been an altogether delightful and rewarding experience. I am especially indebted to Dr. Wiegand, whose contribution to the overall electronics system has helped to make the experiment successful, and to Dr. Ypsilantis for the continuing assistance and guidance he has given me in my research.

It is a pleasure to acknowledge the work done by Mr. Quentin Kerns, Mr. Fred Kirsten, Mr. Dick Mack, Mr. Stanley Baker, Mr. Thomas Nunamaker, and Mr. Arthur Bjerke in the design of circuitry used in this experiment. Mr. Cedric Larson is to be commended for his work in designing the structural support for the "dish" and for supervising its construction. I am grateful to Dr. Geoffrey Chew for many interesting discussions and for his continued interest during the course of the experiment. Thanks are due to Dr. Emilio Segrè for his interest in the work and for many helpful suggestions and to Dr. Herbert M. Steiner for his significant contributions to the initial phases of the work.

Many thanks to the Bevatron Operator Crew for their cooperation and their excellent services. Mr. Frank Corelli deserves special mention for his professional services and his unflinching moral support.

This work was done under the auspices of the U. S. Atomic Energy Commission.

REFERENCES

1. G. F. Chew and F. E. Low, Phys. Rev. 113, 1640 (1959).
2. C. Goebel, Phys. Rev. Letters 1, 337 (1958).
3. Proceedings of the 1960 Annual International Conference on High-Energy Physics at Rochester, (Interscience Publishers, Inc., New York, 1960) p. 638.
4. S. Lindenbaum and R. Sternheimer, Phys. Rev. 109, 1723 (1958).
5. The work was done by Leonard Auerbach, Tom Elioff, William B. Johnson, Joseph Lach, Clyde Wiegand, and Thomas J. Ypsilantis.
6. The 25% estimate was based on the assumption that neutrons would be detected by the recoil protons from n-p collisions in the scintillator.
7. See Joseph Lach, Ph. D. Thesis, Effects of the Single Pion Exchange in the Reaction $p + p \rightarrow p + \pi^+ + n$, University of California, 1962.
8. A. E. Bjerke, Q. A. Kerns, and T. A. Nunamaker, Nucl. Instr. Methods 12, 25 (1961).
9. The buffer-storage and read-out system is described by F. Evans and F. A. Kirsten, Nucl. Instr. Methods 12, 39 (1961).
10. T. G. Innes and Q. A. Kerns, A Pulsed Nanosecond Light Source, Lawrence Radiation Laboratory Report UCRL-9726, Aug. 4, 1961.
11. Arthur E. Bjerke, Quentin A. Kerns, and Thomas A. Nunamaker, Pulse Shaping and Standardization of Photomultiplier Signals for Optimum Timing Information Using Tunnel Diodes, Lawrence Radiation Laboratory Report UCRL-9838, Aug. 30, 1961.
12. S. C. Baker, F. A. Kirsten, D. A. Mack, and C. Wiegand, Nucl. Instr. Methods 12, 11 (1961).
13. Clyde E. Wiegand, Tom Elioff, William B. Johnson, Leonard B. Auerbach, Joseph Lach, and Thomas Ypsilantis, Detection Efficiency of Plastic Scintillator for Neutrons of Energies 4 to 76 Mev, Lawrence Radiation Laboratory Report UCRL-9986, Dec. 14, 1961.

14. S. C. Baker, Q. A. Kerns, F. A. Kirsten, D. A. Mack, and T. A. Nunamaker, Test Routines and Monitoring for a Large Counter Experiment, Nucl. Instr. Methods 12, 1 (1961).
15. Thomas Ypsilantis et al., Phys. Rev. 98, 840 (1955).
16. W. B. Johnson, Ph. D. Thesis, Study of $\pi^- + p \rightarrow \pi^! + \pi^- + n$ at 1.25 and 1.75 BeV/c for Low Nucleon-Momentum-Transfer Collisions: Evidence for Pion-Pion Interactions, University of California, 1962.
17. The pion-carbon cross sections were taken from R. Cool, K. Cronin, and A. Abashian, Phys. Rev. 107, 1121 (1957) and from N. Abbatista, M. Biasco, S. Mongelli, A. Romano, and P. Waloschek, Nuovo Cimento 23, 1 (1962). Pion-proton cross sections were from N. Derado and N. Schmitz, Phys. Rev. 118, 309 (1960).
18. The Monte Carlo calculations for pion rescattering in the dish and for neutron rescattering in the target were done by William B. Johnson and are described in detail in his thesis, University of California, 1962).
19. W. N. Hess, Rev. Mod. Phys. 30, 368 (1958).
20. C. N. Yang and S. B. Treiman, Phys. Rev. Letters 8, 140 (1962).
21. D. L. Stonehill, Ph. D. Thesis, Yale University, 1962.
22. J. Kirz, J. Schwartz, and R. D. Tripp, Phys. Rev. 126, 763 (1962).